

United States Patent Application for

**METHOD AND APPARATUS FOR DECOUPLED THERMO-CATALYTIC  
POLLUTION CONTROL**

Inventors: ALI TABATABAIE-RAISSI  
NAZIM Z. MURADOV  
ERIC D. MARTIN

Attorney Docket No. UCF-226CIP (Continuation-In-Part of  
Provisional Application No. 50/081324 Filed on April 10, 1998  
and of Provisional Application No. 60/107236 Filed on November 5, 1998)

I certify that this correspondence, including the attachments listed, is being deposited with  
the United States Postal Service, Express Mail Post Office to Addressee service,  
receipt No. FJ60253132 US, in an envelope addressed to Assistant Comm.  
for Patents,  
Box Patent Application, Washington, D.C. 20231, on the date shown below.  
4/10/99 \_\_\_\_\_  
Date of Mailing      Signature of Person Mailing

## METHOD AND APPARATUS FOR DECOUPLED THERMO-CATALYTIC POLLUTION CONTROL

This invention relates to processes and apparatus for photocatalytic, thermocatalytic or  
5 combined photo- and thermocatalytic treatment of fluids containing undesirable compounds for  
pollution control and energy production applications and was made with the financial support of  
the U.S. Department of Defense, Naval Surface Warfare Center, Indian Head Division under  
contract number N00174-91-C-0161, Office of Naval Research under Augmentation Awards for  
Science and Engineering Research Training Program, contract number N00014-93-1-0907, and  
10 Army Research Office under Defense University Research Instrumentation Program, contract  
number DAAH04-96-1-0295, and is a Continuation-In-Part of Provisional Application  
60/107,236 filed November 15, 1998, which is a Continuation-In-Part of Provisional Application  
60/081,324 filed April 10, 1998.

### FIELD OF THE INVENTION

Examples of treatable streams include, among others, ventilation makeup air, ambient air,  
air from stripping and off-gassing operations, soil vapor extraction (SVE), airborne matter (*e.g.*  
organic particulate, biogenic and microbial matter) and process vent gas, wastewater treatment off-  
gas, liquid effluents (*e.g.* wastewater, industrial and agricultural runoff) containing at least one  
undesirable or otherwise unwanted compound. Moreover, this application presents a holistic  
20 approach to the design of the high performance photo- and thermocatalytic systems that possess:

- i- Rapid species mass transfer to and from the active sites of the catalyst.
- ii- Uniform transport of thermal and radiant energy to the active sites of the catalyst.
- iii- Decoupling of the conversion efficiency from process intrinsic energy efficiency.
- iv- Minimal pressure drop.

## **BACKGROUND OF THE INVENTION**

As environmental regulations become progressively more stringent, new techniques and approaches are needed for dealing with difficult contaminants. For example, the required destruction and removal efficiencies (DREs) for some environmental pollutants, such as toluene diisocyanate (TDI), dioxin, dibenzofurans and polychlorinated biphenyls (PCBs) are extremely high. Conventional methods such as carbon adsorption or liquid scrubbing are not a complete remediation solution due to the fact that they simply transfer contaminants from one medium (*i.e.* water or air) to another (*i.e.* solid carbon or scrubbing liquid). On the other hand, incineration and catalytic thermal oxidation present their own limitations. For example, the widespread production and use of chlorinated compounds in the industrially developed countries has resulted in large amounts of halogenated organic contaminants to seep into the soil, water and air. Incineration and even thermocatalytic oxidation of wastestreams containing halogenated compounds in many cases produce emission of products of incomplete combustion (PIC) such as dibenzofurans, dioxin and other pollutants that are known or suspected carcinogens. It is to be understood that in the terminology of this application "target species/compounds" denote those entities contained within the contaminated stream that are targeted for complete destruction and removal.

The past two decades has seen rapid growth and promulgation of new remediation technologies. In particular, a class of pollution control technologies known as the advanced oxidation processes (AOPs) has been the focus of much research and development. Among AOPs, those that employ ultraviolet (UV) radiation in conjunction with active oxidants (*i.e.* ozone, hydrogen peroxide, hydroxyl radical, superoxide ion radical, etc.) to accomplish mineralization of the target organic contaminants are of special interest. Generally, UV/AOPs are characterized with respect to the type of either the catalyst and chemical reactions involved (*i.e.* homogeneous vs.

heterogeneous) or light source employed (*i.e.* solar vs. artificial).

In general, UV/AOPs for treatment of the hazardous organic contaminants (HOCs) in fluids (both gas- and liquid-phase) comprise the following steps:

In the first step, an organic contaminant (hereafter-called "primary reactant" or "target compound") that is adsorbed on the catalyst surface or resides within the fluid reacts to form products (hereafter termed "intermediate" or "secondary" products).

In the next step, the secondary products react to form other products (hereafter called "tertiary products" or "final products") that can be regarded as more benign, safer, or less detrimental to health and environment. The tertiary products are formed through a sequence or stepwise reaction scheme and an effective way to obtain tertiary or final products is to use specially engineered catalytic reactors disclosed in this document.

#### **DESCRIPTION OF THE PRIOR ART**

It is generally recognized that the UV-based AOPs do not universally enjoy high process energy efficiencies. This realization has motivated many researchers to test the concept of integrated or hybrid processes. In this approach, several processes are combined to produce a hybrid system that is capable of treating contaminants in the waste stream at much higher overall process energy efficiency and reduced life-cycle costs than each of individual processes, alone. This is especially true in applications where the initial concentration of the target compound may vary wildly in the course of the treatment process.

A good example is ethanol emission (in air) from some pharmaceutical product dryers. Ethanol concentration in the product dryer varies during a typical cycle by two orders of magnitude. Also, hybrid processes can be used in certain applications where valuable chemicals (*e.g.* acrylonitrile monomer, solvents, etc.) are emitted in the effluent that can be recovered. Yet

another example involves treatment of the energetic materials. It is known that the photocatalytic treatment and mineralization of 2,4,6-trinitrotoluene (TNT) in aqueous media is difficult.

However, once partially oxidized, many microorganisms can readily metabolize the partial oxidation products. Here, a UV/AOP is combined with another treatment process (*i.e.* biological) to achieve a much higher process efficiency. Examples of surrogate processes employed in the prior art include bioremediation, electron beam, thermocatalytic oxidation, activated carbon or synthetic adsorbents, UV/H<sub>2</sub>O<sub>2</sub> and UV/O<sub>3</sub>, to name just few. Alternatively, performance improvement can be made at the catalyst/support level, using multifunctional catalytic media, *i.e.* capable of acting as both photocatalyst and thermocatalyst.

It is to be understood that, in the terminology of this application, “media” or “catalytic media” denotes the combination of photocatalyst(s) and its/their supporting base material(s). Most base material(s) of the prior art simply provide(s) a structural support for the active catalyst(s) used and do not normally partake in the reactions or provide other known functions. Examples include, but not limited to, U.S. Patent 4,892,712, 4,966,759 and 5,032,241 to Robertson et al.; U.S. Patent 5,126,111 to Al-Ekabi et al.; and U.S. Patent 5,035,784 to Anderson et al. However, it is possible to have a multifunctional media that is both photocatalytically and thermocatalytically active. The rationale for using a multifaceted media will now be described.

Consider a UV/AOP that employs a high power light source such as a medium-pressure mercury lamp (MPML). MPMLs generate large amounts of thermal radiation, at relatively high temperatures. Even when a low-pressure mercury lamp (LPML) is used as the source of UV light, considerable amount of low-level waste heat is given off. For example, according to vendor specifications, a standard 65 W Voltarc<sup>R</sup> lamp (G64T5VH), converts less than 40% of the input electrical power to emitted light in the form of 254-nm radiation. The electric to UV energy

conversion efficiency is lower yet for fluorescent black light (less than 25%) and medium pressure mercury lamps (less than 15%).

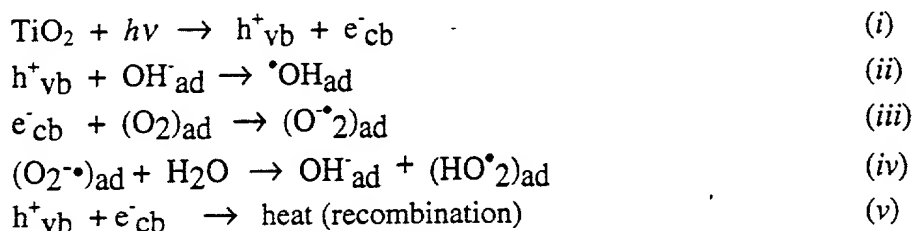
It is generally recognized that only a very thin layer on the photocatalyst surface can actually be excited to enter photocatalytic reactions. For most active photocatalysts, the physical thickness of this layer or skin does not exceed few microns. This is due to the fact that UV radiation is completely absorbed within a skin only few microns thick on the exposed photocatalyst surface. On the other hand, thermal radiation can penetrate deep into the supported catalyst and base material. The fact that most target species can also be adsorbed into the deep layers of the photocatalytic media (inaccessible to UV but affected by thermal radiation and heat) encourages the use of multifunctional catalysts capable of utilizing both heat and light emitted by medium and high pressure UV lamps. Thus, a multipurpose catalyst can comprise a base material that acts as both a thermocatalyst as well as support structure for the photocatalyst. Alternatively, a dual catalyst may be used that can function as both thermocatalyst and photocatalyst, simultaneously. It is also possible to implement a thermocatalyst and a photocatalyst separate but together, in series.

The use of combined photo- and thermocatalytic action as in an integrated media is known in the prior art. Examples include Muradov, N.Z., Tabatabaie-Raissi, A., Muzzey, D., Painter, C.R. and M.R. Kemme, *Solar Energy*, 56, 5 (1996) 445-453; and Fu, X., Clark, L.A., Zeltner, W.A., and M.A. Anderson, *J. of Photochemistry and Photobiology, A: Chemistry* 97 (1996) 181-186, among others. Muradov et al. describe a photo/thermocatalytic method for selective oxidation of airborne volatile organic compounds (VOCs) including nitroglycerin, ethanol and acetone. The light source used was a low-pressure mercury lamp. The catalytic media employed was  $\text{TiO}_2$  modified with silico-tungstic acid (STA) and platinum. Fu et al. describe photocatalytic degradation of ethylene in air at elevated temperatures over sol-gel derived  $\text{TiO}_2$  and platinized

TiO<sub>2</sub> particulates, irradiated with a fluorescent black light lamp. Both studies report improved performance at elevated reaction temperatures without platinization of the photocatalyst.

The use of bandgap semiconductors such as titania (TiO<sub>2</sub>), ZnO, ZrO<sub>2</sub>, CdS, etc. and their various modified forms as the gaseous and aqueous phase photocatalysts is well known in the prior art. For example, TiO<sub>2</sub> particles (anatase crystalline form, in particular) are readily excited upon exposure to near UV radiation (wavelengths below approximately 400 nm) producing electron/hole (e<sup>-</sup>/h<sup>+</sup>) pairs on the semiconductor surface. The recombination of e<sup>-</sup>/h<sup>+</sup> pairs has the resulting effect of reducing the process quantum efficiency. The recombination can occur either between the energy bands or on the semiconductor surface.

It has long been recognized that certain materials such as noble metals (*e.g.* Pt, Pd, Au, Ag) and some metal oxides (*e.g.* RuO<sub>2</sub>, WO<sub>3</sub>, and SiO<sub>2</sub>) facilitate electron transfer and prolong the length of time that electrons and holes remain segregated. The electrons and holes act as strong reducing and oxidizing agents that cause break down of the target compounds via formation of active radicals on the photocatalyst surface. The following groups of reactions describe the excitation of titania leading to the generation of active radicals:



Reaction (a) occurs within the TiO<sub>2</sub> lattice. When TiO<sub>2</sub> absorbs a UV photon, represented by  $h\nu$ , having an energy equal to or greater than its bandgap energy, electrons (e<sup>-</sup><sub>cb</sub>) shift to the conduction band, and positively charged "holes" (h<sup>+</sup><sub>vb</sub>) remain behind in the valence band. Energy is related to wavelength by Planck's equation:

$$E = hc/\lambda$$

Where:  $E$  is the bandgap energy (eV),  $h$  is Planck's constant ( $6.6256 \times 10^{-34}$  Js) and  $c$  refers to the velocity of light ( $2.998 \times 10^{10}$  cm/s), and  $\lambda$  is the wavelength (nm) of radiation.

5 Assuming bandgap energy of 3.1 eV for  $\text{TiO}_2$ , a threshold wavelength of about 400 nm is obtained.  $\text{TiO}_2$  will absorb light having a wavelength equal to or lower than this value. Once holes and electrons are photo-generated they move about the crystal lattice freely in a manner described as the "random walk." The random walk results in the electrons and holes either recombining (thermalizing) per equation (v) or reaching the surface of the catalyst to react with adsorbed species and produce reactive radicals as indicated by equation (ii), (iii) and (iv).

An important factor in controlling the rate of electron-hole recombination on the photocatalyst surface is the size of catalyst particles. The smaller these particles are, the shorter the distance that charge carriers must travel to reach the surface and the larger the exposed catalyst surface area is. Photocatalysts having X-ray diameter of only a few nanometers and BET surface area of many 100s  $\text{m}^2/\text{g}$  are commercially available (e.g. ST-01 and ST-31 grades titania produced by Ishihara Sangyo Kaisha, LTD of Japan).

The rate of recombination of holes and electrons is a function of the catalyst surface irradiance. Prior art teaches that higher the surface irradiance, the greater the rate of recombination of electrons and holes (Egerton, T.A., King, C.J., J. Oil Col. Chem. Assoc., 62 (1979) 386-391). Prior art also teaches that only one of the process (ii) or (iii+iv) is the rate-limiting step. The process involving the other radical completes the reaction and preserves the overall charge neutrality. Thus, it is generally recognized that the hydroxyl radical formation is the rate-limiting step. The rate of surface reactions will then be equal to  $r = k_{(c+d)}[h^+_{vb}]$ . The rate of hole formation is  $k_a q_i$ , where  $q_i$  denotes catalyst surface irradiance (quanta/s/ $\text{cm}^2$ ). The rate of



electron-hole recombination is then  $k_e [h^+_{vb}][e^-_{cb}] = k_e [h^+_{vb}]^2$ . When  $q_i$  is high, a large number of electrons and holes will be generated, and Egerton and King have already shown that:  $r = kq_i^{1/2}$ . At low values of  $q_i$  when surface concentration of holes,  $[h^+_{vb}]$ , is relatively small, the recombination term will be negligible and  $r = k_a q_i$ . The surface irradiance value (hereafter called "Egerton-King threshold") at which the reaction rate transition from  $q_i$  to  $q_i^{1/2}$  (1 to 1/2 dependency) occurs is  $q_{EK} = 2.5 \times 10^{15}$  quanta/s/cm<sup>2</sup> (at  $\lambda = 335, 365$  and  $404$  nm).

The  $q_{EK}$  can be calculated for two commonly used UV light sources (*i.e.* low- and medium-pressure mercury lamps). For the LPMLs and MPMLs  $q_{EK}$  is approximately equal to 1.95 mW/cm<sup>2</sup> (for  $\lambda = 254$  nm) and 1.36 mW/cm<sup>2</sup> (for  $\lambda = 365$  nm), respectively. In order to limit the rate of recombination of electrons and holes and maximize the photoreactor performance, it is necessary to limit the catalyst surface irradiance to levels at or below the Egerton-King threshold. The rate of surface reactions,  $r$ , is proportional to  $q_i^m$ , where  $m$  varies between 1/2 and 1. To increase the rate of surface reactions for target pollutants, it may be necessary to allow  $q_i$  to exceed  $q_{EK}$  under certain conditions. Therefore, in a practical situation, the requirement for an efficient utilization of the photogenerated charge carriers must be balanced against the need for optimum rate of the surface reactions involving the primary and secondary reactants that produce desirable final products. In general, this requires a careful photoreactor design that allows uniform irradiation over all photocatalytic surfaces at a level that is as close to  $q_{EK}$  as possible and optimum rate of conversion of surface-borne target species to desirable final products.

Just like radiation and heat transfer, transport of the primary reactants to and final products from the catalyst surface affect the photoprocess performance. The reactor engineering is closely coupled to the choice and configuration of the media and the type of light source used. A proper photoreactor design should provide for uniform irradiance on all catalytic surfaces as well as

effective species mass transport to and from the catalyst active sites. Mass transfer limitations affect the process efficiency, as all target species must reach the active/activated catalyst surface before any reaction can occur. For process streams containing very low concentration of contaminants, the transport effects are even more pronounced. In general, photoreactor designs  
5 fall into one of the following three categories:

1. Most photocatalytic reactors/processes of the prior art belong in here. The Category I photoreactors possess good mass transfer but generally poor radiation field characteristics.

FIG. 1a, 1b, 1c depict several examples from prior art depicting photocatalyst-coated monolith, photocatalyst-coated panel, and baffled annular photoreactor, respectively. Other  
10 examples include Australian Patent PH7074 to Matthews; U.S. Patent 3,781,194 to Juillet et al.; U.S. Patent 4,446,236 to Clyde; U.S. Patent 4,774,026 to Kitamori et al.; U.S. Patent 4,888,101 & 5,736,055 to Cooper; U.S. Patent 4,892,712, 4,966,759 & 5,032,241 to Robertson et al.; U.S. Patent 5,126,111 to Al-Ekabi et al.; U.S. Patent 5,045,288 to Raupp et al.; U.S. Patent 5,069,885 to Ritchie; U.S. Patent 5,480,524 to Oeste; U.S. Patent 5,564,065  
15 to Fleck et al.; U.S. Patent 5,683,589 to de Lasa et al.; U.S. Patent 5,790,934 to Say et al.; and U.S. Patent 5,030,607 to Colmenares, to name just a few.

2. Poor mass transfer but mostly uniform catalyst surface irradiance, *e.g.* annular photoreactor design (no internals, catalyst coated on the outer wall).

3. Poor mass transfer and non-uniform catalyst surface irradiance, *e.g.* externally lit annular  
20 photoreactor (no internals, catalyst coated on the inner wall).

As noted before, a good photocatalytic reactor design should provide for a uniform near  $q_{EK}$  catalyst surface irradiance and temperature as well as no mass transfer limitations. This requires considerable process and reactor optimization effort prior to scale-up. Experimental

techniques involving the measurement of the radiative properties of materials including photocatalysts are generally very complex and time consuming. Likewise, computational methods for analyzing radiative exchange among surfaces and between surfaces and gases even under the simplest of conditions are very difficult to execute. This so because the equation of transfer, in general, is of the complex integro-differential form and very difficult to solve. Other complexities including chemical reactions, species mass transfer, etc. further complicate photoprocess/reactor analysis and optimization. Therefore, it is not surprising that the prior art offers very little in the way of photocatalytic process and reactor analysis, modeling, optimization and scale-up. When it comes to the photocatalytic reactor and process engineering and design, the prior art methodologies are mostly pseudo-quantitative, semi-empirical and intuitive, in nature.

For example, it has long been recognized that providing means for generating and enhancing turbulence in the flow generally improves species mass transfer to and from the catalyst surface active sites. An examination of the prior art reveals that many articles such as ribs, fins, pleats, beads, chips, flaps, strips, coils, baffles, baskets, wires, etc. have been conceived, used and patented for generating mixing and turbulence in the flow and generally improve mass transfer characteristics of the reactors. Thus, using flow agitating articles or “internals” to enhance the contaminant mass transfer to the catalyst surface is more or less intuitive. But, the effect of internals or “turbulators” on the radiation field within the photoreactor seems to be less obvious and seldom fully appreciated. Often, methods used in the prior art to eliminate mass transfer intrusions adversely affect the extent and uniformity of radiation received on the catalyst surface, within the same photoreactor. One example is the annular photoreactor having internal baffles such as one shown in **FIG. 1c**. The U.S. Patent

5,683,589 (de Lasa et al.), U.S. Patent 5,069,885 (Ritchie), U.S. Patent 5,116,582 (Cooper), and U.S. Patent 5,790,934 (Say et al.) are all variations of this basic configuration. The catalyst surface irradiance for the photoreactor configuration of **FIG. 1c** has been carried out by the subject inventor and results are given in **FIG. 2**.

5 Results of **FIG. 2** indicate that, if internals must be used to improve mass transfer, it is more advantageous to design the photoreactors in such a way that the bulk of catalyst resides on the reactor wall. This requirement limits the number and proximity of internals, in general, and baffles, in particular, that can be incorporated into the photoreactor. It can be seen that for the baffle spacing smaller than one baffle diameter (see U.S. Patent 5,683,589 to de Lasa et al. and U.S. Patent 5,790,934 to Say et al.), the surface irradiance (as a fraction of the lamp's radiosity) is lower on reactor wall than the baffle surface. Furthermore, results of **FIG. 2** indicate that the point of diminishing return with respect to the magnitude and uniformity of the surface irradiance is reached at inter-baffle spacing,  $L$ , of about 10 times the sleeve diameter ( $D_i$ ). The fact that the baffle spacing equal or greater than  $L = 10D_i$  is necessary for achieving a uniform irradiance results in the wall irradiance levels that are well above the  $q_{EK}$ . Moreover, the  $L/D_i = 10$  requirement results in inter-baffle distances that are unsuited to proper fluid mixing. These and other effects combine to make the use of most internals or turbulators generally undesirable.

Another important but poorly understood phenomenon within the photocatalytic reactors of the prior art is the light refraction and reflection effect. **FIG. 3** depicts an annular  
20 photoreactor with three linear UV lamps, 120° apart, along the reactor axis. **FIG. 4a-4b** depict the lateral variation of the wall irradiance as a function of the packing radius,  $r_p$ . All three lamps are lit and data are shown for two  $r_p/r_o$  values (0.333 and 0.452) and a range of baffle spacing, denoted by  $L/r_o$ , from 0.76 to 6.10. On the same graph, the analytical predictions for the lamp as

a diffuse line source emitter are also given. The measured wall irradiance dips at all locations having shortest radial distance to the lamp axis. This effect is due to the refraction and blocking of UV rays from the posterior lamps. When the refraction effects are all accounted for, the experimental data are in good agreement with the analytical and model predictions. This is shown in **FIG. 5** for one of the baffle spacing of the arrangement of **FIG. 4a**, *i.e.*  $L/r_o = 6.10$ . This example clearly shows that refraction and reflection of light is likely to affect irradiance distribution within the catalytic matrix of several photoreactor designs of the prior art such as the U.S. Patent 4,892,712, 4,966,759 & 5,032,241 (Robertson et al.) and U.S. Patent 5,126,111 (Al-Ekabi et al.). It can now be appreciated that the configuration of the catalytic media and design of the photocatalytic and thermocatalytic reactors must be kept as simple as possible. This requirement is in addition to ones discussed before (*i.e.* having good mass transfer and radiation field characteristics).

Moreover, a photoreactor design that yields a uniform irradiance distribution over all its catalytic surfaces, does not lend itself to mass transfer intrusions and has a simple design that is readily scalable, can still be affected by low process energy efficiency. This is so because, in one-pass reactors, the process energy efficiency is coupled with the conversion efficiency (or process DRE). When very high process DREs are required, the transport effects lead to process energy efficiencies that are well below the maximum realizable. This so-called "coupling effect" adds another complexity to the design of high-performance photocatalytic and thermocatalytic reactors. Thus, one object of the present invention is to teach a novel method for mitigating the adverse effects of coupling on the performance and energetics of single-pass photocatalytic, thermocatalytic or combined photo- and thermocatalytic reactors.

An examination of the prior art reveals that six distinct types of catalytic media

arrangement have been used, to date. For the sake of discussions here, they are termed as the Type 0, Type I, Type II, Type III, Type IV and Type V, of which Types 0-II and IV are substantially photocatalytic and Types III and V are substantially thermocatalytic, albeit multifunctional media.

5 In Type 0 photocatalyst/support configuration, a suitable catalyst such as titania is used in colloidal form without any support or base material(s). Examples of Type 0 media include, among others, U.S. Patent 5,554,300 and 5,589,078 to Butters et al.; U.S. Patent 4,888,101 and 5,118,422 to Cooper et al.; and U.S. Patent 4,861,484 to Lichtin. A sub-category of Type 0 media includes, among others, U.S. Patent 5,580,461 (Cairns et al.). Cairns, et al. employ a combined process that includes, in addition to colloidal titania photocatalysis, a surrogate process based on the use of adsorbent material. The contaminated fluid is first contacted with a particulate adsorbent material that physically adsorbs the target compound. The contaminant-loaded adsorbent is then separated from the fluid and brought into contact with aqueous slurry of a suitable photocatalyst. The use of adsorbent material implies, implicitly, that the technique is more suited to treatment of processes in which the adsorption of target species on the photocatalyst surface is the rate-limiting step. This is not generally the case, especially in the vapor-phase processes where the rate of reaction for one or more surface bound species (primary or secondary reactants) control the overall rate of the reaction and final process outcome. It is therefore desirable to simplify the treatment process by eliminating the surrogate adsorbent in  
20 favor of a multifunctional catalytic media (catalyst and support combination) that is both a good adsorbent as well as a good photocatalyst.

In Type I photocatalyst/support arrangement, the catalyst (often a modification of the anatase crystalline form of  $\text{TiO}_2$ ) is immobilized or bonded onto a ceramic, glassy (e.g. fiberglass

mesh, woven glass tape, etc.) or metal oxide (*e.g.* silica gel), metallic (*e.g.* stainless steel), or synthetic polymeric (*e.g.* plastic) substrate. Examples of Type I media include, among others, U.S. Patent 5,564,065 to Fleck et al.; U.S. Patent 5,449,443 to Jacoby et al.; U.S. Patent 5,045,288 to Raupp et al.; U.S. Patent 5,069,885 to Ritchie; U.S. Patent 4,446,236 to Clyde; U.S. Patent 5,736,055 to Cooper; U.S. Patent 5,683,589 to de Lasa et al.; U.S. Patent 5,790,934 to Say et al.; and U.S. Patent 5,374,405 to Firnberg et al.

In Type II media configuration, impregnated glassy mesh/matrix or porous ceramic monolith or beads, metallic and metal oxide substrates (in the form of plates, beads, etc.) are employed as the photocatalyst support to which titania is bonded utilizing a method known as the "sol-gel technique." There are many variations, but, a typical process for preparing colloidal sols and corresponding media is discussed in "Photocatalytic Degradation of Formic Acid via Metal-Supported Titania," H.Y. Ha and M.A. Anderson, J. of Environmental Engineering, March, 1996, pp. 217-18, the contents of which are incorporated herein by reference. First, a solution of titanium isopropoxide mixed with dilute nitric acid in a ratio of  $H_2O/Ti(i-Pro)_4/70\% HNO_3 = 300/30/20$  ml is refluxed at 80 degrees centigrade for 3 days. The resulting colloid is then concentrated with a vacuum rotary evaporator. The final titania concentration of the colloid becomes 1.06 mol/L at pH 0.8. The media support used were stainless steel 304 plates and tin (IV) oxide-covered glass. The stainless-steel plates were pretreated by firing at 450 degrees centigrade for 2 hours to produce a metal oxide layer. A PMW spinner system was used to produce uniform titania layers on the support. The support was spun at 2500 rpm for 30 seconds. The coated gel was first dried at room temperature and then fired at a temperature that may vary between 300 and 600 degrees centigrade with a heating rate of 3 degrees centigrade per minute. Typical dwell times were about 2 hours. The process is repeated until the desired catalyst

thickness is obtained.

Type II catalyst/support examples include, but not limited to, U.S. Patent 4,892,712, 4,966,759 and 5,032,241 all to Robertson et al.; U.S. Patent 5,126,111 to Al-Ekabi et al.; and U.S. Patent 5,035,784 to Anderson et al. In Type I and Type II arrangements, the substrate has  
5 no known function other than providing physical and structural support for the photocatalyst.

Type III catalyst/support configuration is a variation of the Type II media that involves synthesis and use of metal oxide aerogels, most prominently SiO<sub>2</sub> aerogels doped or co-gelled with other transition metal oxides such as titania to produce photochemically active catalyst/support material. There are many methods and variations of the basic technique used for  
10 preparing high porosity metal oxide aerogels. In general, preparation of metal oxide aerogels and porous glasses comprise a two step process in which a condensed metal oxide intermediate is formed. From this intermediate compound aerogels are prepared having any desired density, clarity and UV transparency, thermal insulation capacity, moisture and mechanical stability.

Two general reactions have been used to make earlier metal oxide aerogels. In the process of U.S. Patent 2,249,767 to Kistler, first a metal alkoxide is hydrolyzed by reacting with  
15 water and an alcohol in the presence of a reagent (*e.g.* NH<sub>4</sub>OH). Second, the hydrolyzed metal undergoes a condensation reaction to form a metal oxide gel, from which an aerogel is made by supercritical fluid extraction of the solvents. An improvement to the Kistler's method is given by the single-step sol-gel process of the U.S. Patent 3,672,833 to Teichner et al. Teichner's  
20 method, employs a silicon alkoxide tetramethoxysilane or tetraethoxysilane which is hydrolyzed by one to ten times stoichiometric quantity of water with an alcohol in an acidic, neutral or alkali environment. This is followed by the condensation reaction in which the hydrolysis products polymerize to form a wet gel. In Teichner's method, the alcohol is removed directly from the



wet gel at above supercritical pressure and temperature point of the alcohol. It should be noted that any metal that can form an alkoxide, which includes essentially the entire periodic Table of elements, could be used to make an aerogel. Examples include: silicon, germanium, zirconium, titanium, iron, magnesium, boron, cerium, lithium, and aluminum, to name just few.

5 Further improvement upon the techniques developed by Kistler and Teichner has been made recently through many new syntheses methods. Examples include, among others, U.S. Patent 5,030,607 to Colmenares; U.S. Patent 5,275,796 and 5,409,683 to Tillotson et al.; U.S. Patent 5,538,931 to Heinrichs et al.; U.S. Patent 5,718,878 to Zhang; U.S. Patent 5,759,945 to Carroll et al.; U.S. Patent 5,766,562 to Chattha et al.; and U.S. Patent 5,753,305 to Smith et al. As an example, the properties of the low-density silica aerogels made by method of the U.S. Patent 5,409,683 (Tillotson et al.) is described and incorporated here by reference in its entirety. The density of the silica aerogels prepared by this method varies typically between approximately  $0.0015 \text{ g/cm}^3$  and  $0.8 \text{ g/cm}^3$ . Representative refractive index of the Tillotson silica aerogels are in the range of 1.0005 and 1.170 when measured at a wavelength of 632.8 nm. Light transmittance is typically greater than 85% at 632.8 nm. For a monolithic silica aerogel, 2 cm thick, a bulk density of  $0.05 \text{ g/cm}^3$  and prepared by the method of U.S. Patent 5,409,683, the light transmittance at  $\lambda = 400 \text{ nm}$  is typically 45%. The porosity, expressed as the percentage of open space within the total volume, falls in a range between 64% and 99.9%. The specific surface area of these silica aerogels is in the range of 450 to  $1000 \text{ m}^2/\text{g}$ . The properties of silica  
20 aerogels given here by reference to the U.S. Patent 5,409,683 to Tillotson et al. are also typical of other metal oxide aerogels (*e.g.* titania) prepared by similar techniques.

A typical Type III media most useful to the practice of the present invention can be made by methods of the U.S. Patent 5,409,683 to Tillotson which is incorporated here by reference. In

Tillotson's two-step method, a high purity metal (*e.g.* silicon, titanium, zirconium) alkoxide is mixed with a hydrolysis rate reducing alcohol (such as methanol, ethanol or propanol), an additive (*e.g.* acetylacetone, acetic acid and hydrogen peroxide) and a sub-stoichiometric amount of water to form a solution. If silicon metal is used, the suitable alkoxide is tetramethoxysilane (TMES). Likewise, for titanium metal, the desirable alkoxide is titanium isopropoxide. The metal alkoxide solution is then reacted with a suitable acid catalyst (*e.g.* hydrochloric acid) to form an oligomeric mixture of a partially condensed metal intermediate and a reaction produced alcohol. This is followed by the removal of alcohol by distillation and evaporation. The next step involves adding a nonalcoholic solvent such as acetonitrile or acetone to the partially condensed metal intermediate to form a non-alcoholic solvated condensed metal intermediate which is then reacted with a second catalyst (ammonia or fluoroboric acid) and mixed. The amount of catalyst regulates the pH of the solution and determines the rate of gel formation. After mixing is completed, the condensed metal oxide product is cast, that is, poured into a mold to form a wet gel. The gelation takes about 72 hours and carried out at room temperature. The nonalcoholic solvent and any reaction-generated alcohol is then removed by supercritical extraction using liquefied carbon dioxide, chlorofluorocarbons (freons) or propane. More recently, methods have been developed for preparation of both bulk and thin film aerogels in which the gel drying is carried out under subcritical conditions (Jochen Fricke, "Superexpansive Gels," *Nature*, vol. 374, pp. 409-410, 1995). Another important development involves rapid aging technique for aerogel thin films (U.S. Patent 5,753,305 to Smith, et al.).

An important application of the metal oxide aerogels is their use as heterogeneous catalyst and support structure for chemical processes involving oxidation, epoxidation, hydrogenation, reduction, synthesis, etc. As such, co-gelled metal oxide aerogels such as titania-

silica aerogels and transition metal aerogel-supported catalysts (*e.g.* platinum, nickel, cobalt and copper supported on silica aerogel) are well known in the art. For example, U.S. Patent 5,538,931 to Heinrichs, et al. teaches a process for preparing a supported catalyst comprising a transition metal such as palladium or platinum on an aerogel (*e.g.* silica) that is most useful as a hydrogenation catalyst. U.S. Patent 5,766,562 to Chattha et al. discloses a method for preparing titania aerogel supported precious metal (*e.g.* platinum, rhodium) catalyst useful for the automotive exhaust gas (NO<sub>x</sub>, hydrocarbons and carbon monoxide) emission control. U.S. Patent 5,030,607 to Colmenares teaches a method for preparation of UV light-transparent silica aerogels doped with photochemically active uranyl ions (UO<sub>2</sub><sup>++</sup>) for photocatalytic synthesis of short chain hydrocarbons in a fluidized bed photoreactor.

In Type IV photocatalyst/support media, a photocatalyst (*e.g.* doped and undoped modifications of TiO<sub>2</sub>, CdS, etc.) is deposited by bonding or cementing onto the fabric of a modified or unmodified natural or synthetic polymer material. Examples for polymers of natural origin (or biopolymers) include wood, paper, kozo, gampi, Kraft lignin, and woven cotton, kenaf, linen, wool, etc. (U.S. Patent 5,246,737 to Muradov and U.S. Patent 5,604,339 and 5,744,407 to Tabatabaie-Raissi et al.).

Finally, the Type V media includes the broad field of moderate-temperature (approximately 150-350°C) thermal oxidation catalysts. Of particular interest to practice of the present invention is a sub-class of the moderate temperature thermal oxidation catalysts that include supported transition metal oxide catalysts and cation modified zeolites as dual function sorbent/catalyst media. For example, U.S. Patent 5,414,201 to Greene discloses a combined sorbent/catalyst dual function media which removes dilute VOCs, both halogenated and otherwise, from air at room temperature, and then acts as a catalyst at higher temperatures

(350°C) to both desorb and oxidize trapped VOCs. Due to their microporous crystalline structure, various forms of zeolites like zeolite A (3A, 4A and 5A), Faujasites (zeolites X and Y) and Pentasils (ZSM-5 and Silicalite) have been widely used as commercial adsorbents. Two dual function media, Cr-Y and Cr-ZSM-5 as well as metal-loaded Co-Y zeolite catalyst, prepared by Greene, Prakash and Athota (J. of Applied Catalysis B: Environmental 7 (1996) 213-224), and Ramachandran, Greene and Chatterjee (J. of Applied Catalysis B: Environmental 8 (1996) 157-182), are given below and included here by reference in their entirety.

Cr-Y is made by exchanging  $\text{NH}_4\text{-Y}$  with chromium nitrate solution containing 1.5 gram of chromium nitrate in one liter of distilled water maintained at a pH of 4 for 72 hours.  $\text{NH}_4\text{-Y}$  is prepared by exchanging 15-20 grams of H-Y (LZ-Y-84 from UOP, Si/Al= 2.5, 20 wt% alumina as binder) with 2.24 mol/l ammonium chloride solution for 2 hours. Cr-ZSM-5 is made by exchanging  $\text{NH}_4\text{-ZSM-5}$  with chromium nitrate solution containing 2.3 grams of chromium nitrate in one liter of distilled water at 50°C for 72 hours.  $\text{NH}_4\text{-ZSM-5}$  is prepared by exchanging 15-20 grams of H-ZSM-5 (MFI from UOP, Si/Al= 16, 20 wt% alumina as binder) with 2.24 mol/l ammonium chloride solution. After repeated washing, both exchanged catalysts are dried and subsequently calcined at 500°C. Typical exchanged chromium loading of the Cr-Y and Cr-ZSM-5 catalysts were 0.6 and 0.3 wt%. Typical BET surface area of the Cr-Y and Cr-ZSM-5 dual function catalysts were 474 and 388  $\text{m}^2/\text{g}$ .

To prepare Co-Y, about 20 grams of  $\text{NH}_4\text{-Y}$  is cobalt exchanged with a solution containing 16 grams of  $\text{Co}(\text{NO}_3)_2 \cdot 6\text{H}_2\text{O}$  dissolved in 1l of deionized water. The solution is stirred continuously for 48 hours at 90°C. Typical cobalt loading on the zeolite was 1.5 wt%. After the exchange of all the cobalt ions in the cobalt nitrate solution with  $\text{H}^+$  ions of the zeolite catalyst, the pellets were thoroughly washed with deionized water, dried at 120°C for 2 hours and

then calcined at 500°C for 10 hours. The measured BET surface area of the Co-Y catalyst exceeds 600 m<sup>2</sup>/g of catalyst.

Still another media useful for the practice of this invention has been disclosed by U.S. Patent 5,720,931 to Rossin for catalytic oxidation of organic nitrogen-containing compounds.

5 Typical catalyst composition comprises a noble or a base metal supported on titania (Degussa P-25<sup>R</sup>) or zirconia with added promoters such as molybdenum, tungsten, or vanadium. A typical formulation given by EXAMPLE I of the U.S. Patent 5,720,931 is incorporated here by reference, in its entirety. 25 g of Degussa P-25 titania powder is slurried in 250 ml deionized water. To the slurry is added 2.9 g of lanthanum nitrate hydrate dissolved in 30 ml distilled water. The slurry is placed in a rotary evaporator at 45°C. Water is evaporated from the slurry overnight. The remaining solid is dried at 125°C for 2 hours, then crushed and sieved to 25/60 mesh granules. The granules are then calcined at 450°C, for four hours. Approximately 8 g of this granules are slurried in 200 ml distilled and deionized water. To this slurry is added approximately 0.9 g ammonium metavanadate dissolved in 80 ml distilled and deionized water. The slurry is then placed in a rotary evaporator at 60°C and water is completely evaporated. The remaining solids are then dried at 125°C, for two hours, then calcined at 450°C, for four hours. About 2 g of the resulting granules is slurried in 50 ml deionized water. Then, 0.04 g tetraammineplatinum nitrate dissolved in 25 ml distilled, deionized water is added to the slurry. The slurry is placed in a rotary evaporator at 60°C, and the water is evaporated overnight. The  
20 resulting material is dried at 125°C, for two hours, then reduced in a hydrogen atmosphere for another two hours, at 450°C, then calcined at 450°C, for two hours. The resulting final product contains approximately 1-wt% Pt, 5-wt% V, 5-wt% La, and remaining TiO<sub>2</sub> support.

A further description of photocatalytic patents will now be described:

U.S. Patent 5,790,934 to Say et al. discloses a compact reactor for the photocatalyzed conversion of contaminants in a fluid stream. The reactor includes a support structure with multiple non-intersecting aluminum fins oriented parallel to the general flow direction of the stream. The fins were spray coated with a 1:1 mixture of titanium dioxide photocatalyst and alumina. Several germicidal lamps were inserted into the fins that totaled 148 pieces that were either flat or pleated. The photocatalytic reactor of Say et al. had several alternative designs but all included a large number of flat or pleated fins or baffles at various relative configuration to the light source. Although, it is understood that such a design does present certain advantages with respect to the contaminants mass transfer to the photocatalytic surfaces, it is not at all clear how such configurations can be useful in insuring a uniform irradiance over all catalytic surfaces at or near  $q_{EK}$ . Furthermore, no effort was made to decouple the process energy efficiency from the DRE of the target pollutant (formaldehyde vapor). Also, no references are given to the use of multifunctional photo- and thermocatalytic media of the Type III-V configuration.

U.S. Patents 4,888,101 & 5,116,582 to Cooper and U.S. Patent 5,736,055 to Cooper et al. disclose several titania-based, substantially of the Type 0 slurry photoreactor designs. In one application, a replaceable cartridge for use in a photocatalytic fluid purification is described. The fluid flows through the cartridge in the presence of light. The cartridge includes a flexible; porous element having titania coating associated with it and a rigid support structure. In another embodiment of the invention, a system for photocatalytic modification of a chemical composition comprising substantially titania entrapped within a layer of Pyrex glass wool interposed between two transparent plates. In yet another embodiment, a photocatalytic slurry reactor is disclosed that is driven by solar or artificial UV illumination. A tubular UV lamp is suspended by an O-ring within a cylindrical reactor jacket, creating an annular region through

which a titania slurry is pumped. A helical stainless steel wire wrapped about the bulb acts as a turbulence generator to break up the boundary layer for increased radial mixing.

These processes are substantially Type 0 slurry reactors with generally acceptable mass transfer characteristics but non-uniform irradiance over catalytic surfaces, *i.e.* category I limitation. No effort was made by these researchers to decouple the process energy efficiency from DRE of the target pollutants. Also, no references are given to the use of multifunctional photo/thermocatalytic media of the Type III-V configuration.

U.S. Patents 5,604,339 & 5,744,407 to Tabatabaie-Raissi et al. describe the use of photocatalysts, and in particular titania, as coating on the woody or biopolymeric support materials as an in-situ treatment technique to prevent emission of harmful volatile organic compounds such as formaldehyde,  $\alpha$ -pinene,  $\beta$ -pinene and limonene from emitting surfaces. This invention is strictly an in-situ application and no description is made of ex-situ treatment of airborne contaminants or process vent gases utilizing a photoreactor. No references are given to the use of multifunctional photo/thermocatalytic media of the Type III-V configuration or the use of decoupled media and processes similar to those disclosed here.

U.S. Patent 5,638,589 to de Lasa et al. as previously referenced describes a photocatalytic reactor that requires fiberglass mesh supported photocatalyst wherein only polluted water passes through and treated. The fiberglass mesh is substantially inorganic compound and not a carbon containing synthetic polymeric or biopolymeric material that enhances destruction of pollutants. de Lasa et al. describe no separate series connection of different reactors, nor parallel connections of the reactors, nor different length of catalytic media. Furthermore, the conical baskets do not allow for maximum or uniform collection and distribution of the light source photons. Finally, de Lasa et al. has no teaching for thermocatalytic or combined thermo- and photocatalytic media and

reactor applications. There are no references to decoupling phenomena and means to mitigate that effect in U.S. Patent 5,638,589.

U.S. Patent 5,580,461 to Cairns et al. teaches a process for treating a fluid comprising at least one chemical contaminant. Their purification process involves first contacting the contaminated fluid with a particulate adsorbent material to adsorb the target compound. The contaminant-loaded adsorbent is then separated from the fluid and brought into contact with aqueous slurry of a suitable photocatalyst. The contaminant on the adsorbent material is decomposed to form a product. The product of photocatalytic decomposition is then removed from the adsorbent material and slurry solution. The regenerated adsorbent material and photocatalyst slurry is recycled. The macro-process described by Cairns et al. employs a combined Type 0 process, does not teach a photoreactor design and the approach is substantially different from the reactors/processes disclosed here. There are no references made to decoupling.

U.S. Patent 5,564,065 to Fleck et al. teaches a reaction chamber which is filled with a fine fibrous material capable of holding powdered titania. At the center of the chamber is a source of ultraviolet light. Air containing carbon monoxide is passed through the reaction chamber to be oxidized into carbon dioxide, which then removed out of the filter. An alternative embodiment uses a rectangular plate several feet square containing fibrous material and  $\text{TiO}_2$ . The reactor design for this application is similar to that of U.S. Patent 5,126,111 to Al-Ekabi et al. The process is substantially a Type I media application with the Category I radiation field. No description is given regarding the use of multifunctional photo- and thermocatalytic media having Class III-V configuration. No references are given to the coupling phenomena or methods to deal with that effect.



U.S. Patent 5,374,405 to Firnberg et al. teaches a rotating fluidized bed reactor in which inert solid particles are held in place by centrifugal force. The reactor includes a rotating porous bed drum within a plenum vessel. Gas enters through the walls of the drum and exits at the top. An ultraviolet light source is included within the drum for effecting photochemical reactions. In one embodiment, the solid particles are inert and loaded with reactant, which react with the gas. In other embodiments of this disclosure, the particles do not contain the reactant and reactant is provided within the gas stream. No references are given to the use of medium-pressure mercury lamp in conjunction with the multifunctional photo/thermocatalytic media of the Type III and V. No description of the decoupling of process energy efficiency from contaminants DRE is given. No direct reference to the use of bandgap semiconductor photocatalysts such as titania or use of high-power lamps are disclosed.

U.S. Patent 5,246,737 to Muradov teaches a method for immobilizing a semiconductor or noble metal material on a number of supports including biopolymers. A solution containing methylene chloride and silicone polymer mixed with titania catalyst was used to form slurry. The slurry was applied onto the surface of cotton fiber with a soft brush. No description is given for treating airborne contaminants. Moreover, Muradov does not teach a process or photoreactor to accomplish vapor-phase detoxification. Also, the application of photocatalyst in solution with a solvent containing silicone can adversely affect photocatalyst activity toward oxidative mineralization of environmental pollutants. No references are made to the use of multifunctional photo- and thermocatalytic media of the Type III-V configuration. Also, there is no mention of the use of decoupled media or processes similar to those disclosed here.

U.S. Patents 4,966,759, 4,892,712 & 5,032,241 to Robertson et al. and U.S. Patent 5,126,111 to Al-Ekabi et al. describe methods for immobilizing  $\text{TiO}_2$  and other photoactive

5

20

U.S. Patent 5,045,288 to Raupp et al. describes a technique for removing halogenated volatile and non-volatile organic contaminants from a gaseous stream by mixing with a gaseous

oxygen bearing substance in the presence of a solid metal oxide catalyst, exposed to near ultraviolet (UV) radiation. This patent has a Type I photocatalyst/support configuration. Raupp et al. does not teach a photoreactor design or mention polyfunctional catalysts like those disclosed here. No references to the coupling phenomena and methods to mitigate that are given.

5 U.S. Patent 5,035,784 to Anderson et al. teaches a method for the degradation of complex organic molecules, such as polychlorinated biphenyls on porous titanium ceramic membranes by photocatalysis under ultraviolet light. A special membrane preparation technique known as "sol-gel" process is used. An organometallic titanium compound is hydrolyzed to form a soluble intermediate, which then condenses into the organic titanium polymer. The process includes the preparation of a particulate gel, which is fired to achieve a ceramic material. Anderson et al. note that the control of process parameters is crucial, one important factor being the sintering temperatures at or below 500°C to give a hard dry ceramic. It is not possible, nor desirable to deposit/immobilize ceramic like membranes atop surfaces of polymeric, biopolymeric (*e.g.* wood, paper, etc.) origin subject to the very high sol-gel preparation temperatures that will undoubtedly destroy the substrate. The photocatalyst/support arrangement is substantially Type II configuration. The patent by Anderson et al. does not teach a photoreactor design or mention the use of multifunctional catalysts similar to those disclosed here. No references are made to the coupling phenomena and techniques to mitigate that.

15 U.S. Patent 4,966,665 to Ibusuki et al. describes an application involving vapor-phase, 20 TiO<sub>2</sub>-based photocatalysis of process vent gases containing chlorinated VOCs such as trichloroethylene (TCE) and tetrachloroethylene, is substantially a Type I photocatalyst/support application. No references are made to the use of multifunctional media having Type III-V configuration or the decoupled reactor designs similar to those disclosed here.

U.S. Patent 4,446,236 to Clyde teaches a photochemical reactor which is divided into a first section suitable for containing a volume of fluid and a second section having at least one light transmitting wall. A porous, high surface area, fiber webbing is mounted within the reactor so that a portion of the webbing is immersed in the fluid to be reacted. The webbing moves within the reactor so that the webbing is sequentially immersed in the fluid contained in the first reactor section and then moved to the second reactor section where the webbing and fluid therein are irradiated. This process is substantially a Type 0 application and Category I radiation field design. Furthermore, no reference is given to mitigating the coupling effect present.

U.S. Patent 3,781,194 to Juillet et al. teaches an application involving vapor-phase photocatalysis using  $\text{TiO}_2$  in a manner similar to the U.S. Patent 5,045,288 by Raupp et al. The only difference between this patent and the one described above is that Juillet et al. teach a method for oxidizing hydrocarbons to produce aldehydes and ketones, while, Raupp and Dibble describe a similar method for oxidizing halogenated organic compounds such as TCE.

### **SUMMARY OF THE INVENTION**

A primary object of the invention is to provide a photoprocess and apparatus for an energy efficient mineralization and detoxification of organic pollutants or undesirable chemicals in both gaseous and aqueous streams.

A secondary object of this invention is to provide apparatus and teach methods of treating contaminated fluids using catalysts and energy sources capable of exciting and activating those catalysts. The energy sources capable of exciting and activating the catalysts include, among others, mercury vapor lamps (low, medium and high pressure, blacklight and fluorescent light and actinic), xenon lamps (including xenon-mercury and xenon flashlamp) and halogen lamps. In general, these light sources fall into two distinct classes, namely, low- and high-power lamps. The catalyst can be

a unifunctional, multifunctional or combination of several unifunctional catalysts. Chemical composition, materials of choice and physical configuration of the catalyst is so chosen to be compatible with the choice of the light source and allow its efficient implementation in the decoupled reactors (full and partial) and treatment processes of the present invention. Both low-flux and high-flux media and reactors are based on well-developed principles that include:

- (i) Fluid passage with no mass transfer intrusions.
- (ii) Uniform irradiance over all catalytically active surface layers.
- (iii) Decoupled process energy efficiency from the DRE of target contaminants.
- (iv) Utilization of both photons and process waste heat by using multifunctional media.
- (v) Simple and readily scaleable photoreactor/photoprocess design.

A third object of the invention is to provide an energy efficient photoprocess and apparatus wherein the catalyst is bonded to the fabric of the base material (*i.e.* flexible stocking or rigid, metallic or ceramic screen).

A fourth object of this invention is to construct a flexible base material, hereafter called "stocking" substantially from a natural polymeric (biopolymeric), synthetic polymeric or a combination of both natural and synthetic polymeric material to which a suitable photocatalyst is firmly applied. It is another object of this invention to expose the catalytic stocking to radiation in the range of wavelengths from 184 to 400 nanometers.

A fifth object of the invention is to fabricate the rigid metallic base material, hereafter called "support" substantially from any suitable metal, metal oxide or an alloy such as 316 or 304 stainless steel.

A sixth object of this invention is to surround the light source with either stocking or the support on to which a suitable photocatalytic, thermocatalytic or a combination of photo- and

thermocatalytic material has been deposited, called hereafter "low-flux catalytic media."

A seventh object of the invention is to allow the contaminant stream to pass through the low-flux media, substantially in lateral direction, in a manner that permits retention of the target species within the low-flux catalytic media in a most efficient manner.

5       An eighth object of the invention is to promote full mineralization of the primary (target species) and secondary reactants to innocuous final products. The plurality of a light source radiating at the above-mentioned wavelength range and the low-flux catalytic media surrounding the light source, axisymmetrically, is referred to hereafter "single photocell arrangement".

A ninth object of the invention is to provide a flow regime through the single photocell arrangement that minimizes mass transfer intrusions to the low-flux media.

A tenth object of this invention is to provide an optimum configuration that allows most efficient radiant exchange from the light source to the low-flux media and most uniform catalyst surface irradiance.

10  
15  
20  
25  
30  
35  
40  
45  
50  
55  
60  
65  
70  
75  
80  
85  
90  
95  
100  
105  
110  
115  
120  
125  
130  
135  
140  
145  
150  
155  
160  
165  
170  
175  
180  
185  
190  
195  
200  
205  
210  
215  
220  
225  
230  
235  
240  
245  
250  
255  
260  
265  
270  
275  
280  
285  
290  
295  
300  
305  
310  
315  
320  
325  
330  
335  
340  
345  
350  
355  
360  
365  
370  
375  
380  
385  
390  
395  
400  
405  
410  
415  
420  
425  
430  
435  
440  
445  
450  
455  
460  
465  
470  
475  
480  
485  
490  
495  
500  
505  
510  
515  
520  
525  
530  
535  
540  
545  
550  
555  
560  
565  
570  
575  
580  
585  
590  
595  
600  
605  
610  
615  
620  
625  
630  
635  
640  
645  
650  
655  
660  
665  
670  
675  
680  
685  
690  
695  
700  
705  
710  
715  
720  
725  
730  
735  
740  
745  
750  
755  
760  
765  
770  
775  
780  
785  
790  
795  
800  
805  
810  
815  
820  
825  
830  
835  
840  
845  
850  
855  
860  
865  
870  
875  
880  
885  
890  
895  
900  
905  
910  
915  
920  
925  
930  
935  
940  
945  
950  
955  
960  
965  
970  
975  
980  
985  
990  
995  
1000  
1005  
1010  
1015  
1020  
1025  
1030  
1035  
1040  
1045  
1050  
1055  
1060  
1065  
1070  
1075  
1080  
1085  
1090  
1095  
1100  
1105  
1110  
1115  
1120  
1125  
1130  
1135  
1140  
1145  
1150  
1155  
1160  
1165  
1170  
1175  
1180  
1185  
1190  
1195  
1200  
1205  
1210  
1215  
1220  
1225  
1230  
1235  
1240  
1245  
1250  
1255  
1260  
1265  
1270  
1275  
1280  
1285  
1290  
1295  
1300  
1305  
1310  
1315  
1320  
1325  
1330  
1335  
1340  
1345  
1350  
1355  
1360  
1365  
1370  
1375  
1380  
1385  
1390  
1395  
1400  
1405  
1410  
1415  
1420  
1425  
1430  
1435  
1440  
1445  
1450  
1455  
1460  
1465  
1470  
1475  
1480  
1485  
1490  
1495  
1500  
1505  
1510  
1515  
1520  
1525  
1530  
1535  
1540  
1545  
1550  
1555  
1560  
1565  
1570  
1575  
1580  
1585  
1590  
1595  
1600  
1605  
1610  
1615  
1620  
1625  
1630  
1635  
1640  
1645  
1650  
1655  
1660  
1665  
1670  
1675  
1680  
1685  
1690  
1695  
1700  
1705  
1710  
1715  
1720  
1725  
1730  
1735  
1740  
1745  
1750  
1755  
1760  
1765  
1770  
1775  
1780  
1785  
1790  
1795  
1800  
1805  
1810  
1815  
1820  
1825  
1830  
1835  
1840  
1845  
1850  
1855  
1860  
1865  
1870  
1875  
1880  
1885  
1890  
1895  
1900  
1905  
1910  
1915  
1920  
1925  
1930  
1935  
1940  
1945  
1950  
1955  
1960  
1965  
1970  
1975  
1980  
1985  
1990  
1995  
2000  
2005  
2010  
2015  
2020  
2025  
2030  
2035  
2040  
2045  
2050  
2055  
2060  
2065  
2070  
2075  
2080  
2085  
2090  
2095  
2100  
2105  
2110  
2115  
2120  
2125  
2130  
2135  
2140  
2145  
2150  
2155  
2160  
2165  
2170  
2175  
2180  
2185  
2190  
2195  
2200  
2205  
2210  
2215  
2220  
2225  
2230  
2235  
2240  
2245  
2250  
2255  
2260  
2265  
2270  
2275  
2280  
2285  
2290  
2295  
2300  
2305  
2310  
2315  
2320  
2325  
2330  
2335  
2340  
2345  
2350  
2355  
2360  
2365  
2370  
2375  
2380  
2385  
2390  
2395  
2400  
2405  
2410  
2415  
2420  
2425  
2430  
2435  
2440  
2445  
2450  
2455  
2460  
2465  
2470  
2475  
2480  
2485  
2490  
2495  
2500  
2505  
2510  
2515  
2520  
2525  
2530  
2535  
2540  
2545  
2550  
2555  
2560  
2565  
2570  
2575  
2580  
2585  
2590  
2595  
2600  
2605  
2610  
2615  
2620  
2625  
2630  
2635  
2640  
2645  
2650  
2655  
2660  
2665  
2670  
2675  
2680  
2685  
2690  
2695  
2700  
2705  
2710  
2715  
2720  
2725  
2730  
2735  
2740  
2745  
2750  
2755  
2760  
2765  
2770  
2775  
2780  
2785  
2790  
2795  
2800  
2805  
2810  
2815  
2820  
2825  
2830  
2835  
2840  
2845  
2850  
2855  
2860  
2865  
2870  
2875  
2880  
2885  
2890  
2895  
2900  
2905  
2910  
2915  
2920  
2925  
2930  
2935  
2940  
2945  
2950  
2955  
2960  
2965  
2970  
2975  
2980  
2985  
2990  
2995  
3000  
3005  
3010  
3015  
3020  
3025  
3030  
3035  
3040  
3045  
3050  
3055  
3060  
3065  
3070  
3075  
3080  
3085  
3090  
3095  
3100  
3105  
3110  
3115  
3120  
3125  
3130  
3135  
3140  
3145  
3150  
3155  
3160  
3165  
3170  
3175  
3180  
3185  
3190  
3195  
3200  
3205  
3210  
3215  
3220  
3225  
3230  
3235  
3240  
3245  
3250  
3255  
3260  
3265  
3270  
3275  
3280  
3285  
3290  
3295  
3300  
3305  
3310  
3315  
3320  
3325  
3330  
3335  
3340  
3345  
3350  
3355  
3360  
3365  
3370  
3375  
3380  
3385  
3390  
3395  
3400  
3405  
3410  
3415  
3420  
3425  
3430  
3435  
3440  
3445  
3450  
3455  
3460  
3465  
3470  
3475  
3480  
3485  
3490  
3495  
3500  
3505  
3510  
3515  
3520  
3525  
3530  
3535  
3540  
3545  
3550  
3555  
3560  
3565  
3570  
3575  
3580  
3585  
3590  
3595  
3600  
3605  
3610  
3615  
3620  
3625  
3630  
3635  
3640  
3645  
3650  
3655  
3660  
3665  
3670  
3675  
3680  
3685  
3690  
3695  
3700  
3705  
3710  
3715  
3720  
3725  
3730  
3735  
3740  
3745  
3750  
3755  
3760  
3765  
3770  
3775  
3780  
3785  
3790  
3795  
3800  
3805  
3810  
3815  
3820  
3825  
3830  
3835  
3840  
3845  
3850  
3855  
3860  
3865  
3870  
3875  
3880  
3885  
3890  
3895  
3900  
3905  
3910  
3915  
3920  
3925  
3930  
3935  
3940  
3945  
3950  
3955  
3960  
3965  
3970  
3975  
3980  
3985  
3990  
3995  
4000  
4005  
4010  
4015  
4020  
4025  
4030  
4035  
4040  
4045  
4050  
4055  
4060  
4065  
4070  
4075  
4080  
4085  
4090  
4095  
4100  
4105  
4110  
4115  
4120  
4125  
4130  
4135  
4140  
4145  
4150  
4155  
4160  
4165  
4170  
4175  
4180  
4185  
4190  
4195  
4200  
4205  
4210  
4215  
4220  
4225  
4230  
4235  
4240  
4245  
4250  
4255  
4260  
4265  
4270  
4275  
4280  
4285  
4290  
4295  
4300  
4305  
4310  
4315  
4320  
4325  
4330  
4335  
4340  
4345  
4350  
4355  
4360  
4365  
4370  
4375  
4380  
4385  
4390  
4395  
4400  
4405  
4410  
4415  
4420  
4425  
4430  
4435  
4440  
4445  
4450  
4455  
4460  
4465  
4470  
4475  
4480  
4485  
4490  
4495  
4500  
4505  
4510  
4515  
4520  
4525  
4530  
4535  
4540  
4545  
4550  
4555  
4560  
4565  
4570  
4575  
4580  
4585  
4590  
4595  
4600  
4605  
4610  
4615  
4620  
4625  
4630  
4635  
4640  
4645  
4650  
4655  
4660  
4665  
4670  
4675  
4680  
4685  
4690  
4695  
4700  
4705  
4710  
4715  
4720  
4725  
4730  
4735  
4740  
4745  
4750  
4755  
4760  
4765  
4770  
4775  
4780  
4785  
4790  
4795  
4800  
4805  
4810  
4815  
4820  
4825  
4830  
4835  
4840  
4845  
4850  
4855  
4860  
4865  
4870  
4875  
4880  
4885  
4890  
4895  
4900  
4905  
4910  
4915  
4920  
4925  
4930  
4935  
4940  
4945  
4950  
4955  
4960  
4965  
4970  
4975  
4980  
4985  
4990  
4995  
5000  
5005  
5010  
5015  
5020  
5025  
5030  
5035  
5040  
5045  
5050  
5055  
5060  
5065  
5070  
5075  
5080  
5085  
5090  
5095  
5100  
5105  
5110  
5115  
5120  
5125  
5130  
5135  
5140  
5145  
5150  
5155  
5160  
5165  
5170  
5175  
5180  
5185  
5190  
5195  
5200  
5205  
5210  
5215  
5220  
5225  
5230  
5235  
5240  
5245  
5250  
5255  
5260  
5265  
5270  
5275  
5280  
5285  
5290  
5295  
5300  
5305  
5310  
5315  
5320  
5325  
5330  
5335  
5340  
5345  
5350  
5355  
5360  
5365  
5370  
5375  
5380  
5385  
5390  
5395  
5400  
5405  
5410  
5415  
5420  
5425  
5430  
5435  
5440  
5445  
5450  
5455  
5460  
5465  
5470  
5475  
5480  
5485  
5490  
5495  
5500  
5505  
5510  
5515  
5520  
5525  
5530  
5535  
5540  
5545  
5550  
5555  
5560  
5565  
5570  
5575  
5580  
5585  
5590  
5595  
5600  
5605  
5610  
5615  
5620  
5625  
5630  
5635  
5640  
5645  
5650  
5655  
5660  
5665  
5670  
5675  
5680  
5685  
5690  
5695  
5700  
5705  
5710  
5715  
5720  
5725  
5730  
5735  
5740  
5745  
5750  
5755  
5760  
5765  
5770  
5775  
5780  
5785  
5790  
5795  
5800  
5805  
5810  
5815  
5820  
5825  
5830  
5835  
5840  
5845  
5850  
5855  
5860  
5865  
5870  
5875  
5880  
5885  
5890  
5895  
5900  
5905  
5910  
5915  
5920  
5925  
5930  
5935  
5940  
5945  
5950  
5955  
5960  
5965  
5970  
5975  
5980  
5985  
5990  
5995  
6000  
6005  
6010  
6015  
6020  
6025  
6030  
6035  
6040  
6045  
6050  
6055  
6060  
6065  
6070  
6075  
6080  
6085  
6090  
6095  
6100  
6105  
6110  
6115  
6120  
6125  
6130  
6135  
6140  
6145  
6150  
6155  
6160  
6165  
6170  
6175  
6180  
6185  
6190  
6195  
6200  
6205  
6210  
6215  
6220  
6225  
6230  
6235  
6240  
6245  
6250  
6255  
6260  
6265  
6270  
6275  
6280  
6285  
6290  
6295  
6300  
6305  
6310  
6315  
6320  
6325  
6330  
6335  
6340  
6345  
6350  
6355  
6360  
6365  
6370  
6375  
6380  
6385  
6390  
6395  
6400  
6405  
6410  
6415  
6420  
6425  
6430  
6435  
6440  
6445  
6450  
6455  
6460  
6465  
6470  
6475  
6480  
6485  
6490  
6495  
6500  
6505  
6510  
6515  
6520  
6525  
6530  
6535  
6540  
6545  
6550  
6555  
6560  
6565  
6570  
6575  
6580  
6585  
6590  
6595  
6600  
6605  
6610  
6615  
6620  
6625  
6630  
6635  
6640  
6645  
6650  
6655  
6660  
6665  
6670  
6675  
6680  
6685  
6690  
6695  
6700  
6705  
6710  
6715  
6720  
6725  
6730  
6735  
6740  
6745  
6750  
6755  
6760  
6765  
6770  
6775  
6780  
6785  
6790  
6795  
6800  
6805  
6810  
6815  
6820  
6825  
6830  
6835  
6840  
6845  
6850  
6855  
6860  
6865  
6870  
6875  
6880  
6885  
6890  
6895  
6900  
6905  
6910  
6915  
6920  
6925  
6930  
6935  
6940  
6945  
6950  
6955  
6960  
6965  
6970  
6975  
6980  
6985  
6990  
6995  
7000  
7005  
7010  
7015  
7020  
7025  
7030  
7035  
7040  
7045  
7050  
7055  
7060  
7065  
7070  
7075  
7080  
7085  
7090  
7095  
7100  
7105  
7110  
7115  
7120  
7125  
7130  
7135  
7140  
7145  
7150  
7155  
7160  
7165  
7170  
7175  
7180  
7185  
7190  
7195  
7200  
7205  
7210  
7215  
7220  
7225  
7230  
7235  
7240  
7245  
7250  
7255  
7260  
7265  
7270  
7275  
7280  
7285  
7290  
7295  
7300  
7305  
7310  
7315  
7320  
7325  
7330  
7335  
7340  
7345  
7350  
7355  
7360  
7365  
7370  
7375  
7380  
7385  
7390  
7395  
7400  
7405  
7410  
7415  
7420  
7425  
7430  
7435  
7440  
7445  
7450  
7455  
7460  
7465  
7470  
7475  
7480  
7485  
7490  
7495  
7500  
7505  
7510  
7515  
7520  
7525  
7530  
7535  
7540  
7545  
7550  
7555  
7560  
7565  
7570  
7575  
7580  
7585  
7590  
7595  
7600  
7605  
7610  
7615  
7620  
7625  
7630  
7635  
7640  
7645  
7650  
7655  
7660  
7665  
7670  
7675  
7680  
7685  
7690  
7695  
7700  
7705  
7710  
7715  
7720  
7725  
7730  
7735  
7740  
7745  
7750  
7755  
7760  
7765  
7770  
7775  
7780  
7785  
7790  
7795  
7800  
7805  
7810  
7815  
7820  
7825  
7830  
7835  
7840  
7845  
7850  
7855  
7860  
7865  
7870  
7875  
7880  
7885  
7890  
7895  
7900  
7905  
7910  
7915  
7920  
7925  
7930  
7935  
7940  
7945  
7950  
7955  
7960  
7965  
7970  
7975  
7980  
7985  
7990  
7995  
8000  
8005  
8010  
8015  
8020  
8025  
8030  
8035  
8040  
8045  
8050  
8055  
8060  
8065  
8070  
8075  
8080  
8085  
8090  
8095  
8100  
8105  
8110  
8115  
8120  
8125  
8130  
8135  
8140  
8145  
8150  
8155  
8160  
8165  
8170  
8175  
8180  
8185  
8190  
8195  
8200  
8205  
8210  
8215  
8220  
8225  
8230  
8235  
8240  
8245  
8250  
8255  
8260  
8265  
8270  
8275  
8280  
8285  
8290  
8295  
8300  
8305  
8310  
8315  
8320  
8325  
8330  
8335  
8340  
8345  
8350  
8355  
8360  
8365  
8370  
8375  
8380  
8385  
8390  
8395  
8400  
8405  
8410  
8415  
8420  
8425  
8430  
8435  
8440  
8445  
8450  
8455  
8460  
8465  
8470  
8475  
8480  
8485  
8490  
8495  
8500  
8505  
8510  
8515  
8520  
8525  
8530  
8535  
8540  
8545  
8550  
8555  
8560  
8565  
8570  
8575  
8580  
8585  
8590  
8595  
8600  
8605  
8610  
8615  
8620  
8625  
8630  
8635  
8640  
8645  
8650  
8655  
8660  
8665  
8670  
8675  
8680  
8685  
8690  
8695  
8700  
8705  
8710  
8715  
8720  
8725  
8730  
8735  
8740  
8745  
8750  
8755  
8760  
8765  
8770  
8775  
8780  
8785  
8790  
8795  
8800  
8805  
8810  
8815  
8820  
8825  
8830  
8835  
8840  
8845  
8850  
8855  
8860  
8865  
8870  
8875  
8880  
8885  
8890  
8895  
8900  
8905  
8910  
8915  
8920  
8925  
8930  
8935  
8940  
8945  
8950  
8955  
8960  
8965  
8970  
8975  
8980  
8985  
8990  
8995  
9000  
9005  
9010  
9015  
9020  
9025  
9030  
9035  
9040  
9045  
9050  
9055  
9060  
9065  
9070  
9075  
9080  
9085  
9090  
9095  
9100  
9105  
9110  
9115  
9120  
9125  
9130  
9135  
9140  
9145  
9150  
9155  
9160  
9165  
9170  
9175  
9180  
9185  
9190  
9195  
9200  
9205  
9210  
9215  
9220  
9225  
9230  
9235  
9240  
9245  
9250  
9255  
9260  
9265  
9270  
9275  
9280  
9285  
9290  
9295  
9300  
9305  
9310  
9315  
9320  
9325  
9330  
9335  
9340  
9345  
9350  
9355  
9360  
9365  
9370  
9375  
9380  
9385  
9390  
9395  
9400  
9405  
9410  
9415  
9420  
9425  
9430  
9435  
9440  
9445  
9450  
9455  
9460  
9465  
9470  
9475  
9480  
9485  
9490  
9495  
9500  
9505  
9510  
9515  
9520  
9525  
9530  
9535  
9540  
9545  
9550  
9555  
9560  
9565  
9570  
9575  
9580  
9585  
9590  
9595  
9600  
9605  
9610  
9615  
9620  
9625  
9630  
9635  
9640  
9645  
9650  
9655  
9660  
9665  
9670  
9675  
9680  
9685  
9690  
9695  
9700  
9705  
9710  
9715  
9720  
9725  
9730  
9735  
9740  
9745  
9750  
9755  
9760  
9765  
9770  
9775  
9780  
9785  
9790  
9795  
9800  
9805  
9810  
9815  
9820  
9825  
9830  
9835  
9840  
9845  
9850  
9855  
9860  
9865  
9870  
9875  
9880  
9885  
9890  
9895  
9900  
9905  
9910  
9915  
9920  
9925  
9930  
9935  
9940  
9945  
9950  
9955  
9960  
9965  
9970  
9975  
9980  
9985  
9990  
9995  
10000  
10005  
10010  
10015  
10020  
10025  
10030  
10035  
10040  
10045  
10050  
10055  
10060  
10065  
10070  
10075  
10080  
10085  
10090  
10095  
10100  
10105  
10110  
10115

low-flux media based on the band-gap photocatalysts, *i.e.* single-stage and multi-stage photocatalytic media.

A fourteenth object of this invention is to arrange several of these photocatalytic media, in parallel together, each with its own dedicated ultraviolet light source within an integrated reaction vessel, hereafter called "photocatalytic bank".

A fifteenth object of the invention is to connect/plumb together a number of banks in series to form a "photocatalytic module".

A sixteenth object of this invention is to connect/plumb together a number of photocatalytic modules, in parallel or in series, to form a photocatalytic pollution control "unit" or PPCU.

A seventeenth object of the invention is to arrange and plumb the sub-units of the PPCU in such a manner that either maximizes the overall energy efficiency (apparent quantum efficiency or photoefficiency) of the photocatalytic unit or minimizes the pressure drop across the photocatalytic unit (*i.e.* the difference between the exit port and inlet port pressure).

The subject inventor has determined in the subject invention if a linear light source (*e.g.* a low- or medium-pressure mercury vapor lamp) is used, then the best catalytic media arrangement will be one having a cylindrical (tubular) configuration. Within that configuration, the UV lamp is placed most advantageously along the media axis. It is also desirable to minimize the number of light blocking internals such as baffles, fins, turbulators, pleats, ribs, etc. As such, the active surface of the catalytic media would receive the most uniform irradiance. In the case of high power lamps such as medium- and high-pressure mercury vapor lamps, the type and configuration of the photocatalyst/support (media) is even more critical. This is so because the high power lamps emit radiation and heat at a level orders of magnitude higher than the low-pressure mercury lamps (LPMLs). The output power of a typical commercial LPML is

approximately 1 W/in. On the other hand, medium-pressure mercury lamps (MPMLs) are commercially available with power output of up to 300 W/in, nominal. For the irradiance at the photocatalyst surface to remain at or near  $q_{EK}$ , a minimum distance,  $l_{EK}$ , between the light source and the catalyst surface must be maintained.  $l_{EK}$  is a design parameter and characteristic of the type of UV light source used in the photoreactor. In the case of a tubular catalytic media irradiated with a single low-, or medium-pressure mercury lamp,  $l_{EK}$  is calculated to be approximately 3.8 inches and 68 feet, respectively. For calculating  $l_{EK}$ , the electric to UV light energy conversion efficiency of 0.3 and 0.15 has been assumed for standard LPML and MPML (300 W/in), respectively.

Clearly, based on the  $l_{EK}$  calculations determined by the subject inventor, the implementation of LPMLs as the source of UV radiation in practical photoreactors should not be unusually difficult as long as provisions are made to ensure uniform irradiance over all catalytic surfaces. In other words, LPML-driven systems are generally simpler to design and can accommodate many different types of media and reactor configurations. Thus, the primary consideration in constructing an LPML-based photoprocess is to engineer a uniform irradiance over all catalytic surfaces and design for maximum energy efficiency. The essential feature of such an energy efficient photosystem design is decoupling of the process photo-efficiency from conversion efficiency (or DRE) of the target contaminants. Accordingly, it is an object of this invention to provide a novel and improved LPML-based photocatalytic media (hereafter called "low-flux media") and a photosystem design that is highly energy efficient. The novel features of such a design will be disclosed later in this document.

Unlike, LPML-driven photo-processes, MPML-based systems, as indicated by the  $l_{EK}$  calculation, require large and unrealistic photoreactor dimensions to accommodate both the



photocatalyst and the light source. The requirements of very large catalyst surface area, optimum surface irradiance, uniformity of light distribution and media thermal management in MPML-based photo-processes pose a real design challenge. Therefore, it is clear that most photocatalyst/support materials and media configurations of the prior art are not particularly useful for the MPML-based photoreactors. Thus, another object of the present invention is to provide a new and novel method and process for implementing high power light sources for photo- and thermocatalytic service that is compact and highly energy efficient. The approach is based on the use of transition metal aerogel supported catalytic media and others within a specially designed photoreactor. In the terminology of the present application, MPML-based processes and media hereafter termed as the "high-flux" processes and media.

For high-flux applications, a rotating fluidized bed photoreactor is most desirable. The photocatalytic media is in the form of multifunctional, moderate temperature catalysts of the Type III (*e.g.* metal oxide aerogels, co-gelled metal oxide aerogels including titania-silica aerogels and transition metal aerogel-supported catalysts, etc.) or Type V (*e.g.* supported transition metal oxide catalysts, cation modified zeolites and doped titania catalyst). The reactor consists of a porous rotating drum located within a stationary plenum vessel. The waste stream enters the rotating drum through the porous side wall of the drum and exits from an opening near the top. Rate of the rotation of the drum and amount of solids added and bed thickness is adjusted to minimize bed carry over and maintain operation at or near minimum fluidization condition wherein the bed material expands but few bubbles are formed within the bed. A medium pressure mercury lamp placed within a quartz or fused silica sleeve at the middle and inserted into the photoreactor from the bottom or top. Provisions are made to allow feeding and removal of the photocatalytic media during normal reactor operation, if necessary.

Therefore, other objects of the invention described here are to provide gas-phase photocatalysis and air purification system with very high process quantum efficiency for treating various organic contaminants including: aliphatics, aromatics, halogenated organics, mercaptants, sulfur gases, and others.

Further objects and advantages of this invention will be apparent from the following detailed description of the preferred embodiments, which are illustrated schematically in the accompanying drawings.

### **BRIEF DESCRIPTION OF THE DRAWINGS**

**FIG. 1a** shows a photocatalyst-coated monolith, a Category I design of the prior art.

**FIG. 1b** depicts photocatalyst-coated panels, a Category I design of the prior art.

**FIG. 1c** displays a photocatalyst-coated baffled annular photoreactor, a Category I design of the prior art.

**FIG. 2** shows the variation of wall irradiance for photocatalytic design of prior art depicted in

**FIG. 1c** for the case in which photocatalyst surface emissivity is unity (*i.e.* all UV radiation incident on photocatalyst is absorbed),  $k = D_i/D_o = 0.375$ ,  $D_i = 25$  mm, and 65 W LPML.

**FIG. 3** is the experimental set up for surface irradiance measurements in a clustered tri-lamp photoreactor.

**FIG. 4a and 4b** depict lateral variation of wall irradiance in tri-lamp annular baffled photoreactor. Normalized wall irradiance is given at mid-point between two neighboring baffles for a three lamp cluster (8 W each), lamp radius of  $r_{lamp} = 0.31$ '' and single lamp wall peak irradiance of  $q_{l,\infty} = 3.69$  mW/cm<sup>2</sup>, and packing ratio of **a)**  $r_p/r_o = 0.333$  and **b)**  $r_p/r_o = 0.452$ .

**FIG. 5** shows lateral variation of wall irradiance in tri-lamp annular baffled photoreactor with refraction effects. Normalized wall irradiance is given at mid-point between two neighboring

baffles for a three lamp cluster (8 W each), lamp radius of  $r_{lamp} = 0.31$ " and single lamp wall peak irradiance of  $q_{l,\infty} = 3.69 \text{ mW/cm}^2$ , and packing ratio of  $r_p/r_0 = 0.333$ .

**FIG. 6** depicts the scheme of hydrogen bonding of titania to cellulose polymer.

**FIG. 7a** shows the scanning electron micrograph of Kemira UNITI 908<sup>R</sup> catalyst particles on  
5 cotton (flannel) fibers, according to the subject invention.

**FIG. 7b** shows the scanning electron micrograph of Kemira UNITI 908<sup>R</sup> catalyst particles dispersed on a fiberglass mesh support (PRIOR ART).

**FIG. 7c** shows the scanning electron micrograph of TiO<sub>2</sub> catalyst on fiberglass mesh prepared by the sol-gel technique of U.S. Patent 4,892,712 to Robertson et al. (PRIOR ART).

**FIG. 8a** depicts the air flow and surface irradiance distribution pattern over and within cotton  
10 (flannel) fabric fibers coated with TiO<sub>2</sub> according to the subject invention.

**FIG. 8b** depicts the air flow and surface irradiance distribution pattern over and within fiberglass mesh supported titania in the prior art.

**FIG. 9a** shows a schematic diagram of a single-stage, low-flux reactor configuration of the  
15 subject invention depicting flow of the contaminated stream through the photocatalytic stocking.

**FIG. 9b** shows a schematic diagram of a single-stage, high-flux reactor configuration of the subject invention depicting flow of the contaminated stream through the rotating bed of fluidized photocatalytic particles.

**FIG. 10** depicts photocatalytic oxidation of ethanol in a 1g fluidized bed reactor and a small gap  
20 annular flow reactor.

**FIG. 11a** is a schematic diagram of the single-cell photoreactor application of the subject invention having a single-stage low flux catalytic media (stocking).

**FIG. 11b** is a schematic diagram of the experimental setup for low-flux flow photoreactor tests

of the subject invention.

**FIG. 12** shows experimental flow reactor data for nitroglycerine conversion, obtained in a single photocell equipped with a single-stage cotton stocking of 60 inches long and different diameters. A 60" long low-pressure mercury lamp (Voltarc<sup>R</sup> T64T6) having 65 W nominal power is used.

5 **FIG. 13a** depicts the schematic diagram of a single-cell multi-stage (of unequal lengths) low-flux catalytic reactor of the subject invention for decoupling calculations.

**FIG. 13b** shows a flow chart for determining optimum partitioning ratios of **Fig. 13a**.

**FIG. 14a** shows the schematic diagram of a single-cell equipartitioned (all segments of equal length) low-flux catalytic reactor of the subject invention for decoupling calculations.

10 **FIG. 14b** shows a flow chart for determining performance of single-cell equipartitioned multi-stage catalytic reactors of the subject invention.

**FIG. 14c** shows the schematic diagram of a single-cell equipartitioned (all segments of equal length) high-flux centrifugal fluidized bed catalytic reactor of the subject invention for the decoupling calculations.

15 **FIG. 15** depicts the performance of a single-cell multi-stage equipartitioned (all segments of equal length) catalytic media; Voltarc<sup>R</sup> Model T64T6-VH low-pressure mercury lamp, 60 inches long and 65 W nominal power, flannel cotton fabric as the base material with permeability of 0.075"H<sub>2</sub>O/cps (typical), inlet nitroglycerin (NG) concentration of 10 ppmv, required NG destruction and removal efficiency (DRE) of 99.5%.

20 **FIG. 16** depicts one embodiment of a low-flux, double-stage photocatalytic stocking of the present invention.

**FIG. 17** shows one embodiment of a low-flux, triple-stage photocatalytic stocking of the present invention.

**FIG. 18** depicts experimental vs. predicted performance for low-flux, multi-stage photocatalytic reactors of the present invention.

**FIG. 19a** depicts the schematic diagram of two multi-stage equipartitioned (all segments of equal length) low-flux series catalytic reactors of the subject invention for decoupling  
5 calculations.

**FIG. 19b** shows a flow chart for determining performance of single-cell equipartitioned multi-stage catalytic reactors of the subject invention.

**FIG. 19c** depicts the schematic diagram of two multi-stage (of unequal lengths) low-flux series catalytic reactors of the subject invention for decoupling calculations.

**FIG. 20** depicts the performance of a full-scale photocatalytic pollution control unit (PPCU) of the present invention, having two parallel modules each employing two banks in series and segmented (multistage) cotton (flannel) stockings, for inlet concentration of nitroglycerin  $C_{A0}$  = 10 ppmv, 4" OD photocatalytic stockings, and 60" long LPML (Voltarc<sup>R</sup> T64T6-VH) 65 W nominal power.

**FIG. 21a** depicts the schematic diagram of a two-by-two series-parallel multi-stage equipartitioned (all segments of equal length) low-flux catalytic reactor of the subject invention for decoupling calculations.

**FIG. 21b** depicts the schematic diagram of a two-by-two series-parallel multi-stage (of unequal lengths) low-flux catalytic reactors of the subject invention for decoupling calculations.

**FIG. 22** depicts one embodiment of the present invention's high-flux media and photocatalytic reactor design.

## **DETAILED DESCRIPTION OF THE PREFERRED EMBODIMENTS**

Before explaining the disclosed embodiments of the present invention in detail it is to be

understood that the invention is not limited in its application to the details of the particular arrangements shown since the invention is capable of other embodiments. Also, the terminology used herein is for the purpose of description and not of limitation.

5 The present invention provides a new process for catalytic treatment of contaminants in fluids that is energy efficient, and readily scalable. The process employs catalytic media and an innovative fluid-solid contacting scheme. The performance enhancement is by decoupling of the process energy efficiency from the DRE for target contaminants. The novel features, and specifics of this technique are best demonstrated by an analytical treatise disclosed below. The methodology is for the case of a low-flux photoprocess using photocatalytic media described before. The technique can be used in a like manner to analyze high-flux photoprocess and media of the present.

#### LOW-FLUX PHOTOCATALYTIC MEDIA OF THE PRESENT INVENTION

As far as the low-flux applications are concerned, the best media type and configuration is one that provides the most uniform loading of the undisturbed catalyst onto the base material/support while preserving the optimum catalytic activity. It is to be understood that in the terminology of this disclosure, the low-flux catalytic media of the present invention include photocatalysts and base materials (supports) that operate at or below the process temperature of approximately 100°C. In the preferred embodiment of this invention, the catalytic materials include special multifunctional photocatalysts. Yet, in another preferred embodiment of this invention, the base material is an integral part of or a component of the catalyst material, collectively comprising the low-flux catalytic media. Furthermore, in yet another preferred embodiment of this invention, the catalytic media suitable for use with the low-power UV light source include woven polymeric materials of natural origin (or biopolymers) such as cotton

fabric and most desirably flannel cloth. Since cotton fibers contain a very high cellulose content, the chemical properties are essentially that of the cellulose biopolymer. Cellulose is a long linear polymer of anhydroglucose units  $(C_6H_{10}O_5)_n$  and  $1500 < n < 6000$ . The polymer units are organized into a thread-like structure (elementary fibrils of very long length and approximately 3.5 nm in width). The elementary fibrils are bonded laterally to provide further strength (microfibrils of approximately 10-30 nm long). Each anhydroglucose ring consists of three hydroxyl and two oxygen (- O -) moieties (ring and bridge). Thus, it is possible for the  $TiO_2$  molecules to bind to cotton fibers via following hydrogen bonding (see **FIG. 6**):

- (i)  $\sim Ti = O \bullet \bullet \bullet H - O - CH_2 \sim$
- (ii)  $\sim Ti - O - H \bullet \bullet \bullet O < (\text{anhydroglucose ring}); \text{ by hydroxylated } TiO_2 \text{ surface.}$

This may explain the superior catalyst adhesion to biopolymer fibers and the high degree of catalyst coverage and coating uniformity achieved.

The subject inventor has determined in the subject invention that unaltered natural polymers such as woven cotton cloth and flannel provide an excellent base material/support for bandgap photocatalysts. Biopolymeric materials are superior to other widely used media that include ceramic and woven glass mesh type matrices of the prior art. The low-temperature catalytic media of the present invention, including the integrated titania/biopolymer material, display low pressure drop, excellent stability and contaminant retention. **FIG. 7** depicts the scanning electron micrographs of three catalytic media prepared at the subject inventor's laboratory. **FIG. 7a** shows the Kemira Uniti 908<sup>R</sup> titania immobilized onto a woven cotton cloth, as in the practice of the present invention. **FIG. 7b** depicts a fiberglass mesh support. **FIG. 7c** shows titania deposited by sol-gel technique onto a fiberglass mesh (as in U.S. Patent 4,892,712 by Robertson et al.). Modifications **a**, **b** and **c** are representative of the photocatalyst/support configurations designated as Type IV, Type I and Type II, respectively.

The uniformity and quality of catalyst deposition and dispersion on the woven cotton cloth (flannel) is readily observed. An explanation for the superior performance of the low-flux media of the present invention is given below.

**FIG. 8a** depicts one preferred embodiment of the low-flux media of the present invention comprising TiO<sub>2</sub> particles within the cotton fibers as a Type IV media. **FIG. 8a** and 8b show the likely pattern of fluid flow and light distribution within and around the media of the present invention and glass fibers (media Types I and II of the prior art), respectively. The uniform distribution of the catalyst particles on cotton fibers and relatively large distance between the fibers themselves result in uniform flow and surface irradiance that is superior to that obtained by catalytic media of the prior art (Type I&II). Furthermore, in the Type I and II media:

- (i) Poor catalyst deposition allows bottom layers of the photocatalyst unexposed to UV light and, hence, not participating in the reactions.
- (ii) Non-uniform catalyst coating leads to irregular flow pattern through the mesh.

**EXAMPLES 1 to 3** describe the preferred embodiments of the present invention with respect to preparation of the low-flux media. It is important to note that the following examples detail the best methods known to the applicant at the time of filing this application. It is envisioned that better techniques for the operation and preparation of the catalysts may be developed subsequently and are to be considered as a part of this specification thereof insofar as they come within the scope of the claims.

#### **EXAMPLE 1**

This **EXAMPLE** describes the manner in which one preferred embodiment of the invention's low-flux base material/support was prepared. A rectangular piece of unaltered cotton fabric was machine washed in hot water using a small amount of liquid detergent (*e.g.* Proctor &



Gamble's Tide™), followed by two cold rinses. Then, tumble-dried at 55° C, approximately. The entire process above was repeated for the second time. Fabric's post-wash, fully shrunk dimensions were about 95% of the original, as received dimensions. The rectangular piece of fabric was then sewn along the seam and at both ends into cuffs.

## EXAMPLE 2

This EXAMPLE describes the manner in which one preferred embodiment of the invention's low-flux catalytic media was prepared. The catalyst in the form of titanium hydroxide, TiO<sub>2</sub> or combination of titanium dioxide and titanium hydroxide was added to the synthetic polymeric, biopolymeric or combination of synthetic polymeric and biopolymeric fibers of the base material/support having a concentration in the range of 1-15 percent by weight of the media (base material and catalyst). The preferred form of the titanium containing catalyst material is in the form of commercial compounds marketed under the trade names such as Kemira UNITI-908<sup>R</sup>, Degussa P-25<sup>R</sup>, Hombikat UV100<sup>R</sup>, Bayer Bayertitan 5585<sup>R</sup> and Ishihara ST<sup>R</sup> series (*e.g.* ST-01, ST-11 & ST-31), to name just few.

In one preferred embodiment of the present invention, the catalytic material constitutes titania particles that comprise the crystalline form of anatase or rutile, preferably anatase having BET surface area greater than 45 m<sup>2</sup>/g, preferably greater than 225 m<sup>2</sup>/g; and particle size smaller than 0.1 microns, preferably less than 0.02 microns.

The titanium dioxide particles are firmly bonded to the base material via Van der Waals interaction and hydrogen bonding involving hydroxylated titania surface and OH-groups of the cellulosic anhydroglucose rings. The catalyst is then jet-impregnated into the base material (fabric support) from a pressurized aqueous catalyst slurry solution. The slurry solution was prepared and applied to the fabric by first dry ball milling titania powder so that all particles pass

through U.S. sieve # 60 mesh. Then, admixing 17 grams of catalyst for every 1000 ml of distilled water, preferably, deionized water (Ohmic resistance of 18.5 MΩ). After sonicating each 2L batch of the catalyst slurry solution for approximately one hour, about 50 liters of thoroughly mixed and sonicated catalyst slurry solution was emptied into a glass jar placed upon a magnetic stirrer. Using a PTFE stirring bar, the slurry solution was continuously and vigorously stirred.

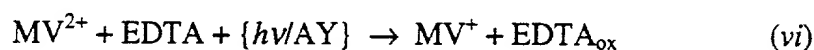
The glass jar containing the slurry solution was then pressurized with nitrogen to about 5 psig. The slurry solution was jet injected, through a ¼ inch PTFE tubing and injector head, onto the inner face of the stocking of EXAMPLE 1. The pre-washed (preferably, machine-washed at least once before sewing and once after), fully shrunk, bone dry, and fully stretched tubular cloth (stocking) was then pulled over a tubular polyvinylchloride (PVC) arm. The cloth covered PVC tube turned slowly as the injector head sprayed the catalyst slurry onto and into the fabric along the PVC arm. Afterwards, the excess fluid was pumped out by squeezing the surface of the fabric, wringing and finally centrifuging for a period of approximately 15 minutes. Then, catalytic stockings were machine dried, eight at a time, at about 55° C, for approximately 30 minutes until bone dry. The catalyst loading on the fabric was determined by weighing fully dried stocking for quality assurance to fall within the range of 0.5 to 1.2 mg of catalyst per cm<sup>2</sup> of fabric surface area. Finally, to provide means for mounting the catalytic stocking within the photocatalytic unit, a Nylon® clamp (e.g. model CX34, by Deflect-O Corp. or SUPERFLEX IN-LINE Nylon 6.6 model IT9115-CO by Panduit Corp.) was inserted into each cuff.

### EXAMPLE 3

This EXAMPLE describes the manner in which other preferred embodiments of the low-flux catalytic media were prepared. Different organic, inorganic and metal-organic additives

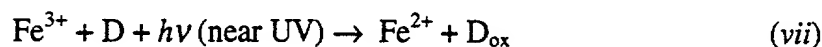
were added to the catalyst slurry of EXAMPLE 2. The solution containing the catalyst and additive was then applied to the base material of EXAMPLE 1. Finally, the supporting base material (fabric) was allowed to dry overnight at room temperature. The preparation method and other details for each additive is given in TABLE I. The rationale for using each additive is disclosed below:

Acridine yellow dye (AY): As an organic dye performs two useful functions: First, being a photocatalyst facilitates various electron transfer reactions (*e.g.* photogeneration of hydrogen from aqueous solutions of electron donors). Second, as a photosensitizer extends the absorption properties of the base material/support of semiconductor-based photocatalysts. Acridine yellow is one of few organic dyes that perform both functions. For example, prior art (Muradov, N.Z., et al. Reaction Kinetics and Catalysis Letters, v.3/4, 1981, 355) teaches that AY is an effective photocatalyst for the visible light (450-500 nm) induced photoreduction of methylviologen ( $MV^{2+}$ ) in the presence of organic donor EDTA with the quantum yield of 56%, according to (vi)

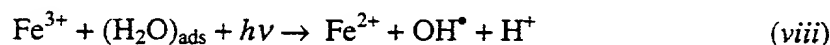


Another advantage of using AY as a co-catalyst and sensitizer for  $TiO_2$  is its relatively high resistance to oxidation.

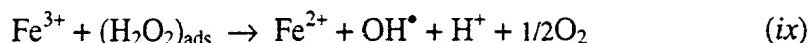
$Fe(NO_3)_3$ : Prior art teaches that  $Fe^{3+}$  ion is a powerful photo-oxidant when exposed to near-UV radiation in aqueous solution, according to (vii)



Where, D and  $D_{ox}$  is the original and oxidized form of the organic compound, respectively. OH-radicals can be produced from  $Fe^{3+}$  by either light reaction with adsorbed water molecules, as in (viii):



or by intermediate  $\text{H}_2\text{O}_2$  formed via dark reaction (ix):



Partial hydrolysis of  $\text{Fe}(\text{NO}_3)_3$  can form  $\text{Fe}_2\text{O}_3$  that will remain on the titania surface and as the prior art teaches (Ibusuki, T., and K. Takeuchi, J. Molecular Catalysis, 88, 1994, 93) can act as a co-catalyst with  $\text{TiO}_2$  in various photooxidation processes (e.g. photooxidation of  $\text{NO}_2$  to  $\text{HNO}_3$ ).

Platinum (Pt): The main function of Pt as a co-catalyst is its ability to mitigate electron transfer reactions by forming a reservoir for electrons. Presence of Pt colloids on the titania surface can potentially facilitate and prolong separation of the photogenerated electrons and holes thus increasing the overall efficiency of the photoprocess. Also, Pt can catalyze the oxygen reduction process for producing peroxoradicals as in (x):



Peroxoradicals can be the source of additional hydroxyl radicals, the main active species in oxidative destruction of organics, thus (xi):



Platinum can also catalyze undesirable reactions, for example, the termination of OH-radicals via formation and decomposition of hydrogen peroxide according to the following reactions: (xii), (xiii), and (xiv)



Activated carbon (AC): The rationale for using super-activated carbon (surface area 250  $\text{m}^2/\text{g}$ ) as an additive to  $\text{TiO}_2$  is to enhance the mass-transfer characteristics of the catalyst/support structure by increasing the surface area of the media. Apparently, once NG is adsorbed on the

AC surface it diffuses to the titania surface thus increasing NG local concentration and, thus, increasing the apparent quantum efficiency. However, it is very important to employ an optimum AC/TiO<sub>2</sub> ratio, because at high AC/TiO<sub>2</sub> ratios, AC is likely to adversely affect the system efficiency by depriving TiO<sub>2</sub> surface from useful photons.

5        NaOH: Prior art (Samorjai, G., in Photocatalysis: Fundamentals and Applications, N. Serpone and E. Pelizzetti (Editors), Wiley Interscience, NY, 1989, 251) teaches that alkali hydroxides (KOH or NaOH) catalyze the hydroxylation of oxide semiconductors (e.g. SrTiO<sub>3</sub>) surfaces and thus, facilitate certain photocatalytic processes (e.g. water dissociation). Since the rate of OH-radical photogeneration is a function of the concentration of surface hydroxyl groups, then it is plausible that hydroxylation of the titania surface can affect kinetics of photooxidation.

TABLE I

Photocatalyst (g)	Additive (wt%)	Volume of slurry (ml)	Preparation details
DP (20.45)	None	300	Slurry
DP (5.74)	None	750	Slurry
DP (10.34)	None	400	Slurry
H-UV (10.50)	None	400	Slurry
KU (10.50)	None	350	Slurry
SrTiO <sub>3</sub> (11.00)	None	600	Slurry
KU (12.01)	None	700	As received dyed (red) fabric
KU (12.00)	AY (0.41)	500	100 ppm by weight Acridine yellow solution
KU (12.00)	NaOH (45.83)	500	Added 100 ml of 5.5 wt% NaOH solution
KU (12.00)	Fe(NO <sub>3</sub> ) <sub>3</sub> (16.67)	500	Added 100 ml of 2 wt% of Fe(NO <sub>3</sub> ) <sub>3</sub> solution
Pt/KU (12.00)	Pt (1.82)	500	46 ml of 1 wt% H <sub>2</sub> PtCl <sub>6</sub> diluted in 100 ml of water, purged with H <sub>2</sub> at 60°C for 3 hrs
KUXA (12.00)	None	600	Slurry
KUXA (12.00)	AY (0.41)	500	Added 100 ppm by weight Acridine yellow to solution
KU (12.00)	Saffron (1.50)	750	0.18 g of crushed Saffron in H <sub>2</sub> O added to KU slurry
DP (12.0)	AC (15.00)	750	1.8 g of activated carbon AX-21 added to DP slurry

Where: DP- TiO<sub>2</sub> (Degussa P25), KU- TiO<sub>2</sub> (Kemira Uniti 908), H-UV- TiO<sub>2</sub> (Hombikat UV100), KUXA- TiO<sub>2</sub> (Kemira Uniti XA067), AY- Acridine yellow dye, AC - activated carbon.

Finally, particular choice of the catalyst also depends on the specific application involved.

For example, when chlorinated compounds (*e.g.* trichloroethylene, TCE) are treated, hydrochloric acid is often formed as one of the final products. The chloride ion bonds strongly to the noble metals such as platinum and palladium when present in combination with TiO<sub>2</sub>, SiO<sub>2</sub>, or SiO<sub>2</sub> supported TiO<sub>2</sub>. It has been observed that the noble metal deactivates quickly under these  
5 conditions due to the strong affinity of the chloride ions for noble metals.

Iron (Fe) as a transition metal can exist in two stable oxidation states, *i.e.* Fe<sup>2+</sup> and Fe<sup>3+</sup> and can catalyze reduction of halogenated organics. But, in a moist environment with excess oxygen, iron oxide forms leading to the catalyst inactivation. However, in a combined metal and metal oxide-supported noble metal catalyst, the SiO<sub>2</sub> support of the high-flux media (or carbonaceous substrate of the low-flux media) adsorbs target species and thus partakes in the catalytic action of the photocatalyst (TiO<sub>2</sub>). As the charge carriers are formed on the light activated titania, electrons migrate to the surface of the photocatalyst, to be trapped by the noble metal. The negatively charged noble metal reduces Fe<sup>3+</sup> to Fe<sup>2+</sup>. Then, Fe<sup>2+</sup> is oxidized back to Fe<sup>3+</sup> by the chlorinated compounds at the surface. The process continues without the noble metal or transition metal oxide deactivation. As such, TiO<sub>2</sub> harvests the incoming photons converting them to charge or charge  
10 equivalent. As noted before, the noble metal acts as a mediator to transfer the charge or charge equivalent to target organic species.

Therefore, it should be understood that in the preferred embodiments of this invention each element or the oxide of each element is an integral part of the catalytic media. Alternatively, iron  
20 can mediate the charge transfer to the platinum when the interaction between Fe and titania is such to preferentially cause charge transfer to Fe upon TiO<sub>2</sub> illumination. Therefore, a synergism exists and can be described for other noble metals and their oxides including Ru, Rh and Ag and other semiconductors such as SnO<sub>2</sub>, SrTiO<sub>3</sub>, WO<sub>3</sub>, Fe<sub>2</sub>O<sub>3</sub>, CdS, ZnO, Ta<sub>2</sub>O<sub>5</sub>, ZrO<sub>2</sub> and CdSe.

## HIGH-FLUX PHOTOCATALYTIC MEDIA OF THE PRESENT INVENTION

As far as the high-flux applications are concerned, the preferred media type and configuration is one that provides highest catalytic activity at the lowest media temperature. It is to be understood that in the terminology of this disclosure, the high-flux catalytic media of the present invention include the plurality of the catalyst and base material (support) that operate in the temperature range of approximately 150-400° C. In the preferred embodiment of the present invention, the high-flux media is silica, alumina or combination thereof with well-defined framework and structural features as in zeolites, zeolite-like materials as well as the synthetic aerogel materials.

In the preferred embodiment of this invention, the catalytic materials including the multifunctional Type III (combined photo- and thermocatalyst) and Type V (combined sorbent and thermocatalyst) media are used. Yet, in another preferred embodiment of this invention, the base material is an integral part of or a component of the catalyst material, collectively comprising the high-flux catalytic media.

In one embodiment of the invention, the catalytic media suitable for use with the high-power UV light sources (*e.g.* medium-pressure mercury lamps) also include the UV-transparent silica aerogels doped with photochemically active compounds (*e.g.* TiO<sub>2</sub>). It is yet another preferred embodiment of this invention to utilize as the high-flux media, co-gelled metal oxide aerogels such as titania-silica aerogels and transition metal aerogel-supported catalysts (*e.g.* platinum, nickel, cobalt and copper supported on silica aerogel).

In another preferred embodiment of this invention, the catalytic media composed of chromium- and cobalt-exchanged zeolite-Y and chromium-exchanged ZSM-5 (molecular sieve) is used. Yet, in another embodiment of this invention, multifunctional catalysts such as the noble

or base metal supported on  $\text{TiO}_2$  or  $\text{ZrO}_2$  and doped with one or more promoters chosen from the group of elements: Mo, W, V, and La, is used.

#### RATIONALE OF THE INVENTION

Among UV/AOTs, titania-based processes are of particular interest since they generally do not require added or otherwise consumable chemicals. Volumes have been written on the efficacy of UV-excited titania and other bandgap photocatalysts for treatment of organics in water and air. Despite all that, to date, no commercially viable UV/ $\text{TiO}_2$ -based pollution control device has been successfully mass-marketed. This is particularly true for applications involving aqueous-phase photocatalytic treatment. A review of the prior art reveals many reasons cited as the stumbling blocks to successful implementation of pollution control devices based on UV-excited,  $\text{TiO}_2$  and other bandgap photocatalysts. A short list of the generally recognized impediments include:

- Practical problems and poor economics of employing slurried colloidal titania in aqueous-phase applications.
- Mass transfer limitations associated with processes that employ immobilized instead of slurried colloidal  $\text{TiO}_2$ .
- Mass transfer limitations affecting treatment of dilute contaminated streams.
- Non-uniform irradiance over catalytic surfaces and light transmission limitations within photocatalytic reactors of the prior art.
- Higher costs when added oxidants are used in both slurried and immobilized titania-based processes.

As noted before, an important consideration is the overall energy efficiency of the photocatalytic service. Due to cost and performance considerations, most detoxification applications require single pass, continuous flow of the contaminant stream. Most photoreactors of



the prior art are not able to utilize UV photons effectively, especially when very high DREs are required. This is a manifestation of the "one-pass or single-pass" process requirement that greatly limits the overall apparent process quantum efficiency (photoefficiency). It is generally recognized that, even under the best of conditions (i.e. no mass transfer limitations present and uniform catalyst surface irradiance) only a fraction of the maximum energy efficiency realizable can be obtained. This is especially true when the process DRE required is high. The net effect of this loss of process photoefficiency is to raise both the operating and capital costs of the photocatalytic treatment. This is so because generating photons capable of exciting the photocatalyst requires costly electricity and use of special UV lamps having electric to UV light energy conversion efficiency of no more than 35%, at best.

Therefore, it can be said that not until an engineering approach is found to eliminate this limitation, it is unlikely that UV photocatalysis can be implemented, widely, as a viable and cost-effective pollution control technology. Thus, it is the object of the present invention to substantially improve upon performance of the catalytic treatment process by:

- (i) Devising a catalytic process that is unaffected by mass transfer intrusions.
- (ii) Ensuring the most uniform irradiance distribution over all catalytic surfaces.
- (iii) Implementing specially designed and formulated catalytic media and process configuration that allow decoupling of the process energy efficiency from DRE of the target pollutants.
- (iv) Employing multifunctional media that allow combined photocatalytic and thermocatalytic activity, whenever desirable.
- (v) Simplifying photoreactor and photoprocess optimization and scale-up.

Now, the theoretical basis of the subject invention that guided the development of the

present innovative photosystem designs is disclosed by considering the axisymmetrical configuration 1a and 1b of **FIG. 9a** and **9b**. The catalytic media of the subject invention comprising the low-flux media 20-a can be supported photocatalyst, supported thermocatalyst or a multifunctional media that is both photocatalyst and thermocatalyst. In a like manner the high-flux media 20-b is a fluidized particle bed that can be supported photocatalyst, supported thermocatalyst, or a multifunctional media that is both photocatalyst and thermocatalyst. In the preferred embodiments of the present invention, the low- and high-flux media (20-a and 20-b) are the Type IV and Type III (or V), respectively. The low-flux reactor in one embodiment of this invention consists of a tubular cell 10-a in which the light source 30-a is placed concentrically along the axis, within a protective quartz or fused silica sleeve 30-c. In thermocatalytic or high-flux case, a heat source 30-b (such as a medium pressure mercury lamp, a heated coil or element, etc.) is placed along the axis and within a quartz or fused silica sleeve 30-c, as before. It is noted that, in the description that follows, the choice of an axisymmetric media is for the sake of illustrating the application of the preferred embodiments of this invention. The procedure described below is also applicable to media configurations having non-circular cross section (*e.g.* rectangular, elliptical, rippled, etc.).

Referring to configuration 1a of **FIG. 9a**, 10-a refers to an impermeable hollow shell (metallic, synthetic polymeric, *i.e.* DuPont's TYVEK<sup>R</sup> and the like), having a closed end 12-a and opposite open-end passageway 14-a, about a closed mid portion 16-a. A permeable catalytic media 20-a (Type IV catalytic material coated onto cotton flannel, synthetic polymeric cloth or woven glass fiber cloth/mesh) has one end 22-a connected to shell closed end 12-a, and opposite end 24-a, connected to shell mid portion 16-a. Stream A passes into inlet 19-a, passes through the catalytic media 20-a and out end passageway 14-a.

1 In a like manner, referring to configuration 1b of **FIG. 9b**, 10-b refers to an impermeable  
rotating drum (*i.e.* metallic, and the like), having a closed end 12-b and opposite closed end 16-b  
about an open mid portion passageway 14-b. The impermeable rotating drum 10-b housed  
within a stationary plenum vessel 10-c, closed at both ends 6 and 8. A permeable rotating grid or  
5 distributor 18 holds the fluidized particle bed 20-b (Type III or V catalytic media). In the  
preferred embodiment of this invention, rotating grid 18 is fabricated in the form of a truncated  
cone with a 2-8° taper angle, more preferably about 4° taper angle. Furthermore, the rotating  
grid 18 is constructed using at least a 22 gage perforated sheet metal having at least 50% open  
area. The inside surface of the grid 18 is covered with a U.S. Sieve #100 mesh stainless steel  
screen butt-welded to perforated basket at either side and tightly wrapped on the outer surface  
with one layer of a close-knit glass fiber mesh/cloth. The rotating basket or grid assembly 18 has  
one closed end at 22-b connected to impermeable rotating drum closed end 16-b, and opposite  
end 24-b, connected at mid portion to fused silica sleeve 30-c. Stream A passes into inlet 19-b  
through the stationary inlet conduit 21 into the space between rotating plates 12-b and 24-b,  
15 through permeable rotating grid 18, passes through fluidized catalytic media 20-b and out end  
passageway 14-b, through stationary exit conduit 23. The rotating drum 10-b is supported at the  
bottom and top by ball (or roller) bearings 25 and 27, respectively. Additional bearings 29 and  
31 are provided at the bottom and top to support rotating fused silica sleeve assembly 30-c.  
Special fluid-tight seals are also provided at the interfaces between the rotating and stationary  
20 articles at 33, 35, 37 and 39. The UV lamp 30-b is stationary, so are the connecting power leads  
41 and 43. The lamp coolant (air or nitrogen) enters at 50 through rotating metallic (*e.g.*  
stainless steel) inlet tubing 40 and exits at 55 through the rotating metallic (*e.g.* stainless steel)  
outlet tubing 45. Finally, the gear system 65 delivers the torque 60 developed by an electrical

motor to gear 70 connected to the rotating inlet conduit 75.

The fluid containing contaminant A enters the catalytic media 20-a in **FIG. 9a**. It flows radially outward through the catalytic media and then along the reactor axis, in the space between the catalytic media and reactor wall, and out of the reactor at the opposite end. In a like manner, the contaminated stream enters the high-flux reactor radially through the grid and centrifugal fluidized particle bed and exits the reactor axially at one open end of the rotating drum. Both the low-flux and high flux reactors of **FIG. 9a** and **9b** can operate either horizontally or vertically, independent of direction of gravitational acceleration.

It is understood that the analysis disclosed below is equally valid if the direction of the flow that enters and exits the low-flux reactor is reversed (*i.e.* contaminated stream entering the catalytic media from the dark side of the photosystem). In certain applications, it is desirable or advantageous to have the contaminant stream flow in crossing the catalytic media from the space between the catalytic media and reactor wall (dark side) to the space between catalytic media and heat/light source (light side). One example is when the incoming flow contains dust, particulate matter, or compounds detrimental to the catalyst activity. In the case of high-flux reactor, the fluid containing contaminant A must always enter the high-flux catalytic media of **FIG. 9b** from the dark side of the rotating particle bed. Finally, it should be noted that the analysis below follows the same line of logic regardless of whether a low-flux or a high-flux reactor is present, or whether or not the target species cross the light side to the dark side or vice versa. Now let:

In **Fig. 9a** and **9b**,  $Q_I$  refer to flow rate of contaminated stream A.

$C_{A0}$  be inlet concentration of target pollutant A.

$C_{Af}$  be exit concentration of target pollutant A.

$D_0$  be the mean diameter of the low-flux catalytic media 20-a in **Fig. 9a** or high-flux catalytic media 20-b in **Fig. 9b**.

$dV$  be low- and high-flux incremental volume for analysis.

$L$  be the length of low-flux media 20-a in **Fig. 9a** or height of the high-flux fluidized catalytic media 20-b in **Fig. 9b**.

$z$  be the coordinate distance from inlet 19-a in Fig. 9a or the closed end of the rotating basket/grid 24-b in Fig. 9b.

$dz$  be the incremental length of the control volume being analyzed in Fig. 9a and 9b.

5 Furthermore, let's consider an irreversible surface reaction on the catalytic media.

Assuming steady state conditions prevail, the material balance for species A in the elemental reactor volume  $dV$  can be written as

$$-Q_I \frac{dC_A}{dz} = (-r_{AS}) = \text{rate of disappearance of reactant A} \quad (1)$$

10

Where  $Q_I$  is the volumetric flow rate (actual),  $C_A$  is the bulk concentration of species A, and  $r_{AS}$  refers to the rate of reaction of species A on the catalyst surface. The rate of the reaction,  $r_{AS}$ , expressed per unit mass of catalyst, may be written either in terms of the diffusion rate from the bulk fluid to the catalyst surface or in terms of the rate on the surface as follows:

$$(-r_{AS}) = k_m a_L (C_A - C_{AS}) = k_{AS} \delta' C_{AS}^p (\alpha q_i)^m \quad (2)$$

Where;

$C_{AS}$  = concentration of species A on the catalyst surface

$k_m$  = mass transfer coefficient from fluid to catalyst surface

$k_{AS}$  = reaction rate constant per unit mass of catalyst

$a_L$  = mass/heat transfer area per unit length of the catalytic media

$\delta'$  = Mass of catalyst per unit length of the catalytic media

For radial/lateral flow through catalytic media, it can be said that,  $k_{AS} \delta'$  is very much less than  $k_m a_L$ . Under these conditions, the mass transfer resistance is negligible with respect to the surface reaction rate, i.e., the kinetics of the surface reaction control the rate. Then,  $C_{AS}$  approaches  $C_A$  in the bulk fluid, and the rate is

$$(-r_{AS}) \approx k_{AS} \delta' C_A^p (\alpha q_i)^m \quad (3)$$

30

In equation (3), the term  $(\alpha q_i)^m$  represents the photonic contribution to the reaction rate of species A on the photocatalytic surface. In the case of a purely thermocatalytic media, equation (3) reduces to

$$(-r_{AS}) \approx k_{AS} \delta' C_A^p \quad (4)$$

Exponent  $p$  and  $m$  represent reaction orders with respect to the concentration of species A and photons capable of exciting the photocatalyst. Clearly, in certain situations, the assumption that  $C_{AS} = C_A$  may not be valid. In those situations  $C_{AS}$  is determined in terms of the bulk concentration of species A. The rate of consumption of pollutant A on the surface of the catalyst can then be described by the Langmuir-Hinshelwood-Hougen-Watson (LHHW) formulation. For example, if the reaction at the surface is irreversible, involves only species A and product P of the reaction is very strongly adsorbed but adsorption of the reactant A is relatively weak, then, the rate equation becomes:

$$(-r_{AS}) = k'_{AS} \delta' C_A / C_P$$

Another example is when the reacting molecules, intermediate products (or secondary reactants) or final reaction products are strongly adsorbed on the surface. This is the case when treating plasticizers such as diethylphthalate (DEP) or di-n-propyladipate (DPA). Oxidation of DEP and DPA on the surface of titania proceeds by way of phthalic acid (PA) and adipic acid (AA), respectively, as the intermediate products. PA and AA are strongly adsorbed on the catalyst surface. However, if the oxidant is present in excess or the concentration of pollutant A is low, and all other contaminants present adsorb very weakly, then, equation (3) is valid and  $p \approx 1$ . From equation (1) and (3), we have

$$Q_1 \frac{dC_A}{dz} = -k_{AS} \delta' C_A (\alpha q_i)^m \quad (5)$$

Equation (5) is solved, subject to the following boundary conditions:

$$C_A = C_{A0} \text{ at } z = 0; \text{ and, } C_A = C_{Af} \text{ at } z = L$$

to yield

$$\frac{C_{Af}}{C_{A0}} = \exp \left[ - \frac{k_{AS} \delta' L (\alpha q_i)^m}{Q_1} \right] \quad (6)$$

Where;  $C_{A0}$  and  $C_{Af}$  refer to the bulk fluid concentration of species A at the reactor inlet and outlet and L is the reactor/catalytic media length. In terms of conversion,  $x_m$ , equation (6) can be rewritten to give

$$x_m \equiv 1 - \frac{C_{Af}}{C_{A0}} = 1 - \exp\left[-\frac{k_{AS}\delta' L(\alpha q_i)^m}{Q_i}\right] \quad (7)$$

The apparent quantum efficiency of the photo-process,  $\phi_i$ , is defined as

$$\phi_i \equiv \frac{(-r_{AS})}{\pi D_0 \alpha q_i} \quad (8)$$

Where

$q_i$   $\equiv$  irradiance on the catalytic surface

$\alpha$   $\equiv$  absorptivity of photocatalyst material

$D_0$   $\equiv$  mean diameter of the catalytic media 20-a or 20-b in **Fig. 9a** and **Fig. 9b**, respectively, as before.

Here,  $r_{AS}$  is defined as the rate of reaction per unit length of catalytic media. Then,

substituting for  $(-r_{AS})$  from equation (3) into equation (8) and noting:  $p = 1$ , we have

$$\phi_i \equiv \frac{k_{AS}\delta' C_A (\alpha q_i)^{m-1}}{\pi D_0} \quad (9)$$

At the onset,  $\phi \equiv \phi_0$  and  $C_A \equiv C_{A0}$ , so that

$$\phi_0 \equiv \frac{k_{AS}\delta' (\alpha q_i)^{m-1} C_{A0}}{\pi D_0} \quad (10)$$

or

$$k_{AS}\delta' (\alpha q_i)^m = \frac{\pi D_0 \alpha q_i \phi_0}{C_{A0}} \quad (11)$$

Substitute from equation (11) into equation (6) and (7) to get

$$\frac{C_{Af}}{C_{A0}} = \exp\left(-\frac{\phi_0 \alpha W_{uv}}{Q_i C_{A0}}\right) \quad (12)$$

and

$$x_m = 1 - \exp\left(-\frac{\phi_0 \alpha W_{uv}}{Q_i C_{A0}}\right) \quad (13)$$

Where,  $W_{uv} = \pi D_0 q_i$  refers to the ultraviolet (all wavelengths at or below that needed to excite the photocatalyst) power output of the lamp 30-a in **Fig. 9a** or 30-b in **Fig. 9b**. Now, let

$$\eta \equiv \frac{\alpha W_{uv}}{Q_1 C_{A0}} \quad (14)$$

5 Then, equation (12) and (13) can be rewritten as

$$\frac{C_{Af}}{C_{A0}} = \delta_f = \exp(-\eta \phi_0) \quad (15)$$

Where, by definition:  $\delta_f = C_{Af}/C_{A0}$ , and then

$$x_m = 1 - \exp(-\eta \phi_0). \quad (16)$$

10 The process photo-efficiency  $\phi$  can be expressed in terms of  $\phi_0$ , as

$$\frac{\phi_1}{\phi_0} \equiv \frac{\frac{k_{AS} \delta_f}{\pi D_0} (\alpha q_i)^{m-1} C_{Af}}{\frac{k_{AS} \delta_f}{\pi D_0} (\alpha q_i)^{m-1} C_{A0}} = \frac{C_{Af}}{C_{A0}} \equiv \delta_f$$

Then

$$\frac{\phi_1}{\phi_0} \equiv \frac{C_{Af}}{C_{A0}} \equiv \delta_f \equiv 1 - x_m \quad (17)$$

Thus

$$\phi_1 \equiv \phi_0 (1 - x_m) = \phi_0 \delta_f \quad (18)$$

Equation (17) and (18) imply that in a single-stage low- and high-flux photocatalytic reactors 1a of **FIG. 9a** and 1b of **Fig. 9b**, the single-component conversion efficiency  $x_m$  is always coupled to the apparent process photo-efficiency  $\phi_1 (= \phi_0 \delta_f)$ . The "coupling" equation 18 also implies that as the process DRE  $\rightarrow 100\%$  (*i.e.*  $x_m \rightarrow 1$ ), the single-stage photoefficiency approaches zero ( $\phi_1 \rightarrow 0$ ). This is an inherent deficiency of the photocatalytic processes that results in lower and lower photo-efficiencies (poor energetics) at increasingly higher and higher process DREs. A method for mitigating this effect and, thus, decoupling  $\phi_1$  from  $x_m$ , constitutes the essence of the present invention, disclosed in the following pages. From equation (16), write



$$\frac{dx_m}{d\eta} = \phi_0 \exp(-\eta\phi_0) \quad (19)$$

Combining equation (18) and (19) gives

$$\phi_1 \equiv \frac{dx_m}{d\eta} \equiv -\frac{d\delta_f}{d\eta} = \phi_0 \delta_f$$

Also

$$\phi_1/\phi_0 = (dx_m/d\eta)/(dx_m/d\eta)_{at \eta=0} = 1-x_m = \delta_f \quad (20-a)$$

Alternatively, the generalized form of the coupling equation can be written as

$$\phi_1/\phi_0 = (d\delta_f/d\eta)/(d\delta_f/d\eta)_{at \eta=0} = 1-x_m = \delta_f \quad (20-b)$$

Finally, for purely thermocatalytic media, combining equation (4) to (7) gives

$$x'_m \equiv 1 - \exp\left[-\frac{(-r_{AS})_{\max} L}{Q_1 C_{A0}}\right] \quad (21)$$

Where,  $(-r_{AS})_{\max}$  refers to the maximum value of thermocatalytic reaction rate that is

$$(-r_{AS})_{\max} = k'_{AS} \delta' C_{A0} \quad (22)$$

and

$$k'_{AS} \equiv A \exp\left(\frac{E}{R_g T}\right) \quad (23)$$

Where,  $A$  is the frequency (or pre-exponential) factor and  $E$  is the activation energy.  $R_g$  refers to ideal gas constant.

Noting that, surface ("heterogeneous") Damkohler member,  $Da$ , is defined as

$$Da \equiv \frac{(-r'_{AS})L}{Q_1 C_{A0}} \quad (24)$$

Then, equation (21) can be rewritten as

$$x'_m \equiv 1 - \exp(-Da). \quad (25)$$

For the general case wherein the catalyst media 20-a of **Fig. 9a** and 20-b of **Fig. 9b** may

be active as either photocatalyst or thermocatalyst, combining equation (16) and (25) yields

$$x_m = 1 - \exp [-(\eta\phi_0 + Da)] \quad (26)$$

Equation (26) represents the general case of the photocatalytic, thermocatalytic or

5 combined photo- and thermocatalytic process conversion efficiency subject to no mass transfer limitations. Equation (26) can be rewritten as

$$x_m = 1 - \delta_f = 1 - \exp [-(\eta\phi_0 + Da)]$$

where, as before

$$10 \quad \delta_f = \frac{C_A}{C_{A0}} \quad (27)$$

Then

$$15 \quad \delta_f = \exp [-(\eta\phi_0 + Da)] \quad (28)$$

From equation (14)

$$20 \quad \eta = \frac{\alpha W_{uv}}{Q_1 C_{A0}} = \frac{a}{Q_1 C_{A0}} = aH \quad (29)$$

Where

$$25 \quad H = \frac{1}{Q_1 C_{A0}} \quad (30)$$

and

$$30 \quad Da = \frac{(-r'_{AS})L}{Q_1 C_{A0}} = (-r'_{AS})LH \quad (31)$$

Then

$$35 \quad 1 - x_m = \delta_f = \exp [-(\eta\phi_0 + Da)] = \exp [-(a\phi_0 - r'_{AS}L)H] \quad (32)$$

In equation (32), "a" is a parameter whose value depends on the units of  $Q_1$ ,  $C_{A0}$ , and  $W_{uv}$  as well as the type of light source employed.  $Q_1$ ,  $C_{A0}$  and  $W_{uv}$  are given in units of  $Ls^{-1}$ , ppmv and mW, respectively. In equation (32), "a" is equal to 1062 and 122,543 for typical low-

pressure mercury lamp 30-a (60 inch arc length and 32% electric to photon energy efficiency) and medium-pressure mercury lamp 30-b (60 inch arc length, 200W/in output and 20% electric to photon,  $\lambda < 400$  nm energy efficiency), respectively. Again, equation (32) represents conversion for the general case of a photocatalytic, thermocatalytic or combined photo- and thermocatalytic process that is

- 1- Free from mass transfer intrusions.
- 2- Provides uniform catalytic media surface irradiance
- 3- Results in a uniform catalyst temperature.

The coupling equation (20) now takes the following form:

$$x_m = 1 - \delta_f = 1 - (dx_m/dH)/(dx_m/dH)_{at H=0} \quad (33)$$

Again, equation (33) applies if the photocatalytic or thermocatalytic process is free from the mass transfer intrusions and all catalytic surfaces are uniformly irradiated or heated. The low- and high-flux catalytic media/processes of the present invention all conform to the requirements of equation (32) and (33), as depicted by the following examples.

#### EXAMPLES 4 & 5

EXAMPLES 4 and 5 describe the low-flux data obtained by the subject inventor using small-gap annular and fluidized bed photocatalytic reactors. These EXAMPLES are intended to show that if, by design, no mass transfer intrusions exists within photoreactor; then, equation 32 describes species conversion, regardless of the reactor type and fluid-solid contacting scheme.

EXAMPLE 4 refers to small gap annular reactor tests. The reactor body was a Pyrex<sup>R</sup> tube having 38 mm outside diameter and a nominal length of 90 cm. A standard, Voltarc Tubes, Inc. G36T6 germicidal low-pressure mercury vapor lamp was placed co-axially within the Pyrex tube. Titania (Degussa P25) wash coated onto the inner surface of the photoreactor. The reactor

volume was 808 ml; flow passage (gap between the inner wall of the reactor and quartz sleeve encasing LPML) was 3.5 mm and catalyst geometrical surface area totaled 1531 cm<sup>2</sup>. Air stream containing 845 and 85 ppmv ethanol vapor entered the annular photoreactor. All reactor walls were kept at a constant temperature of about 85° C.

5       EXAMPLE 5 refers to a standard 1 g (acceleration of gravity, 9.8066 m/s<sup>2</sup>) fluidized bed (1gSFB) photoreactor tests. The bed materials consisted of fine silica-gel particles that provided the base material for titania photocatalyst. The photocatalyst was deposited on the silica-gel particles by soak & dry technique. After wash coating silica particles, they were baked at 450° C for several hours before use. The catalyst loading for these tests was approximately 20-wt%.  
10       The packed bed thickness for EXAMPLE 5 tests were about 11 mm and mean particle size fell in the range of 100-120 mesh (U.S. standard sieve sizes). The expanded bed volume was measured to be approximately 15.3 ml. The diameter of the quartz grid (distributor) was 40 mm. The fused silica fluidized bed tube was placed inside a photon bucket surrounded by six 8W low-pressure mercury lamps. LPMLs could be turned on in banks of 2, 3, 4, and 6 lamps.

15       **FIG. 10** depicts ethanol conversion results for the low-flux flow photoreactor of EXAMPLES 4 and 5. It can be seen that ethanol conversion data obtained within the small gap (3.5 mm) annular and 1g fluidized bed (11 mm thick particle bed) photoreactors closely conform to the plug flow approximation given by equation 32. In a like manner, all the low-flux catalytic media and photoreactors of the present invention also conform to plug-flow approximation given  
20       by equation (32) and (33). This will be demonstrated by EXAMPLES 7-12, later in the text. But first, we disclose the preferred embodiments and design criteria for the single-stage, high-flux rotating fluidized bed reactors of the present invention as follows.

## EXAMPLE 6

The governing equations for designing the preferred high-flux rotating fluidized bed reactors of the present invention are as follows:

$$\Delta P_{FB} = m_{B1} \omega_0^2 / 2\pi L \quad (34)$$

$$Ga = \left[ \frac{150(1-\varepsilon_B)}{\varepsilon_B^3 \phi_S^2} \right] Re_{MF} + \frac{1.75}{\varepsilon_B^3 \phi_S} Re_{MF}^2 \quad (35)$$

$$Q_1 = \rho_f u_1 A_{grid} = \rho_f u_1 \pi D_0 L \quad (36)$$

Where;

$$Ga = \text{Galileo Number} = \left( \frac{\rho_s}{\rho_f} - 1 \right) \omega_0^2 D_0 \frac{\overline{d_p^3}}{v_f^2} \quad (37)$$

$$Re_{MF} = \text{Reynolds Number} = \frac{u_{MF} \overline{d_p}}{v_f} \quad (38)$$

In equations 34 to 38,  $\Delta P_{FB}$ ,  $m_{B1}$ ,  $\omega_0$ ,  $\varepsilon_B$ ,  $\phi_S$ ,  $\rho_s$ ,  $d_p$ ,  $\rho_f$ ,  $v_f$ ,  $u_{MF}$ ,  $u_1$ ,  $D_0$ ,  $L$ , and  $A_{grid}$  denote catalyst bed pressure drop, single-stage fluidized bed mass, angular velocity of the grid/basket, bed void fraction, sphericity of catalyst particle, particle density, mean particle diameter, fluid density, fluid kinematic viscosity, minimum fluidization velocity, superficial fluid velocity at grid surface, diameter of rotating grid/distributor, bed height, and grid surface area, respectively. The minimum fluidization velocities in centrifugal fluidized bed reactors are based on a correlation given by equation (36) due to Levy, E.K., Martin, N. and J.C. Chen, *Fluidization*, Edited by F. Davidson and D.L. Kearins, Cambridge University Press, London, p.71 (1978), which is incorporated herein by reference.

General guidelines for designing high-flux, multi-stage centrifugal fluidized bed photocatalytic, thermocatalytic and combined photo- and thermocatalytic reactors of the present

invention based on the equations above are as follows:

1. Process conditions are so chosen to facilitate plug-flow behavior for species transported across the particle bed. This requires that the superficial fluid velocity to remain near minimum fluidization velocity  $u_{MF}$  all the time. In the preferred embodiment of this invention,  $u_f$  varies between 2 and 4 times  $u_{MF}$ . For reactor throughputs much beyond  $4u_{MF}$ , the extent of bubble formation and fluid by-pass is considerable.
2. With reference to equation (34), it is important to have large  $L$  but small  $m_{B1}$  and  $\omega_0$ . Large  $L$  also favors irradiance on the bed surface (refer to FIG. 2 and note large  $L/D_i$ ). The requirement for small bed mass can also be satisfied in most cases. Considering limited penetration of UV light across fluidizing particle bed of mostly opaque catalyst material, an expanded bed thickness of approximately 5-20 mm (depending on the mean particle diameter, bed void fraction, etc.) is normally sufficient. Bed angular velocity is related to reactor throughput via equation (35).

### EXAMPLE 7

EXAMPLES 7 to 12 describe the preferred embodiments of the present invention with regard to the low-flux catalytic media implementation at single cell, plurality of multiple cells (or banks) and unit (multiple banks) levels. FIG. 11a and 11b depict one preferred embodiment of the low-flux catalytic media implementation of the present invention wherein the catalytic process occurs within a single tubular metallic cell 110. With reference to FIG. 11a, the main reactor body 110 is constructed from seamless 6061-T6 (aerospace grade) aluminum tube, 4.5" OD x 4.0" ID x 60" long (LL). Two 6.0" diameter aluminum end caps 116 and 118 are bolted to two aluminum flanges 112 and 114, respectively. The aluminum flanges 112 and 114 are welded to either end of the reactor tube 110. The end caps not only seal the reactor tube, but also

provide a means for installation of the photocatalytic stocking as well as the devices necessary for monitoring of the process variables (pressure, temperature, irradiance, etc.). The irradiance levels within the reactor are measured in two locations using an International Light, model IL1700/SED005 radiometer 140. Radiometer 140 measures 254 nm radiation with 120-volt power supply 147. Radiometer was mounted parallel to the lamp axis facing a quartz window 141 installed on the inlet end cap 116. Pressure drop across the photocatalytic stocking is measured with a differential pressure gauge 144 (Dwyer Magnehelic) connected with 1/8" OD PTFE tubing to two static pressure taps 153 and 155 attached to the reactor end caps 116 and 118, respectively.

The preferred light source for this embodiment is a standard low-pressure mercury vapor lamp such as one commercially available from VTI, *e.g.* G64T5VH having 120 volt power supply 131. The ultraviolet light source 130 is placed within a 1" OD quartz or fused silica sleeve 132 that is closed in one end. The quartz sleeve 132 is mounted along the axis of the phototube via a bushing assembly located on the exit end cap 118 as depicted in **FIG. 11a**. The open end of the quartz sleeve 132 protrudes from the exit end cap 118 to accommodate lamp's electrical connections and cooling line 133. Lamp cooling is accomplished by directing dry cooling air 133 (provided by an Ingersoll-Rand compressor model SSRXF50SE 137, **FIG. 11b**). Typically, 1.5 SCFM of air is fed through a 1/4" OD PTFE tubing 134, that extends half way into the quartz sleeve 132 providing the necessary cooling to the UV lamp. This flow of air was sufficient to maintain lamp's cold spot temperature within the optimum range and around approximately 51°C. The lamp's cold spot temperature is measured by a type "K" thermocouple 135 attached to the lamp envelope at 139, halfway along its length. Reactor outer wall temperature is monitored with a thermocouple pasted onto the outer shell, half way down its

length. Temperature monitor 136 gives the skin temperature of the catalytic stocking 120 via thermocouple 145 (attached to the fabric at 149) and lamp 130 envelope temperature via thermocouple 135 (attached to the lamp at 139).

Referring to **FIG. 11a**, catalyst/support (base material) 120 of the present invention  
5 comprised of a tubular cotton fabric onto which a suitable photocatalytic material has been deposited according to teachings of EXAMPLE 3 and Table I. In one preferred embodiment of the present invention, the low-flux media 120 is comprised of the woven cotton flannel fabric. Catalytic media 120 connects at one end 122 to flange 112 and has an opposite end 124 connected to an impermeable PTFE end baffle 129. A reagent mixing chamber 158 is used to prepare vapor-phase contaminant stream A as depicted in **FIG 11b**. Reagents are loaded into two Hamilton<sup>TM</sup> gas-tight syringes 154a and 154b as depicted in **FIG. 11b**. All syringes have shanks and plungers that are preferably glass and PTFE construction, respectively. The syringe volume (capacity) depends on the carrier gas flow (e.g. air) and varies between 1 to 50 ml. Fully loaded syringes are then placed on a KD Scientific syringe pump 160 that pumps reagents (e.g. a mixture of nitroglycerine and acetone as depicted in **FIG. 11b**) to a Sonics and Materials<sup>TM</sup> brand ultrasonic atomizer probe 152 via a 1/16" OD PTFE tubing as depicted in **FIG 11b**. The atomizer probe 152 is bolted to a stainless steel plate 156 that covers the open end a glass bell jar 150 of the mixing chamber 158 as shown in **FIG. 11b**.

The mixing chamber 158 comprised of an inverted glass bell jar 150 supported at the top  
20 by a stainless steel plate 156 and a round donut-shaped aluminum ring 157. The heated carrier gas such as air enters at the top of the mixing chamber through a 1/2" OD stainless steel tube 162. The atomized liquid is mixed with the carrier gas and delivered to the reactor via a 1" OD heated stainless steel line 163. The mixing chamber wall temperature and the gas within are



measured using type "K" thermocouples 166 and 164, respectively as shown in **FIG. 11b**. A static pressure tap 170 at the top of the mixing chamber allows gas pressure measurement.

Now, with reference to **FIG. 11b**, dry compressed air from 137 enters the system through two mass flow controllers 172 and 174 (Porter, model 204A). One portion of the metered air (typically 10 SCFM) passes through air heater 176 (Omega, model AHP-7561) and then into the mixing chamber 158. The second portion of the metered air (typically 10.15 SCFM) passes through second air heater 178 (Omega, model AHP-7561) and after by-passing the mixing chamber 158, combines with and dilutes its exit flow as depicted in **FIG. 11b**. The combined stream enters into the photocatalytic reactor 110 at A1. According to **FIG. 11a**, air containing contaminant A passes into one end of catalytic media 120 about lamp 130 and then in the direction of arrow A2 through sides of catalytic media 120 and into the space between 120 and reactor wall 110 at A3 and exit out of the reactor at A4.

An isokinetic sampling probe 180 is installed just upstream of the reactor as depicted in **FIG. 11b**. Gas collected by the probe passes through a Tenax adsorbent tube (Supelco 35/60, Orbo #42) and through a rotameter 184 (Gilmont Accucal) for quantification. Typical sampling volume is 27 liters, collected at about 1.8 L/min for 15 min. The reactor effluent is sampled via 182 and 186, as depicted in **FIG. 11b**, in a manner similar to that described above for the reactor inlet stream. The sampling flow rate at the exit is lower than that at the inlet due to lower exit port pressure. A portion of the exit gas is diluted with air (31:1) and then fed to a chemiluminescence NO<sub>x</sub> analyzer 186 (TECO, model 42) for real time monitoring of NO and NO<sub>2</sub> concentrations. NO<sub>x</sub> data is acquired using a PC based data acquisition system 188 (Workbench PC, Strawberry Tree, Inc.) as shown in **FIG. 11b**.

The EPA method 5 and OSHA method 43 (or NIOSH-2507 method) are employed,

wherever applicable, to sample and analyze the inlet and outlet reagent concentration. The less volatile organic compounds are trapped within absorbent tubes supplied by Supelco company. Isokinetic sampling probes are used with the less volatile compounds. The analytical system consists of a capillary gas chromatograph (GC), connected to a Varian Saturn II ion-trap mass spectrometric system. The GC column used is a J&W fused silica capillary column, 15m long, 1/4 mm ID, with 1 micron coating of DB-1. Fixed gases and volatile organic compounds are analyzed on a packed column (30 feet, 1/8" OD Hayesep D<sub>B</sub>) using Varian GC 3400 equipped with flame ionization and thermal conductivity detectors.

#### EXAMPLE 8

The article of EXAMPLE 7 wherein the reagent solution was 5% by weight nitroglycerin (NG) in acetone (DMK). The carrier gas was heated air (approximately 85°C) flowing at 8 standard cubic feet per minute (SCFM). The average outside diameter of the catalytic stocking 120 used was 3.5 inches.

#### EXAMPLE 9

The article of EXAMPLE 7 wherein the reagent solution contained 5% by weight nitroglycerin in acetone. The carrier gas comprised of air heated to 90°C and flowing at 8 SCFM into the mixing chamber 158 and photocatalytic reactor 110 (FIG. 11b). The material of the catalytic media or stocking 120 was woven cotton duck fabric, having an OD of 2.75 inches.

#### EXAMPLES 10 to 12

The article of EXAMPLE 7 wherein the reagent solution contained 2-nitrodiphenylamine (2NDPA) stabilized nitroglycerin. The reagent delivery system was a U-shaped glass tube packed with glass wool and filled with a mixture of NG and 2NDPA solution. The carrier gas was heated air at 90° C flowing at 8, 10 and 12 SCFM corresponding to EXAMPLES 10, 11,

and 12, respectively. The low-flux media (catalytic stocking) 120 was woven cotton flannel (both sides brushed) having an OD of 3.75 inches.

### EXAMPLE 13

This Example demonstrates the performance of a single-stage photocatalytic stocking (SSPCS). Base material/support for this SSPCS was super flannel cotton, having an OD of about 3.8 inches, prepared according to the teachings of EXAMPLE 1. The catalytic media of this example was Kemira UNITI-908 prepared according to instructions of EXAMPLE 2 with no additives or further modifications. The SSPCS was prepared in a manner described in EXAMPLE 3. The SSPCS was tested in the low-flux reactor of FIG. 11 according to the methods and procedures described in EXAMPLE 7 and 9. Briefly, the reagent solution used contained 5% by weight nitroglycerine in acetone. The carrier gas comprised of air heated to about 95°C and metered at 15.5 SCFM (approximately 20.2 ACFM at the average reactor temperature) entering into the reagents mixing chamber 158 and then into the photocatalytic reactor 110 (FIG. 11b). Concentration of nitroglycerin in the gas-phase was approximately 9.0 ppmv. The nitroglycerine DRE measured at approximately 75% ( $\approx 79.5\%$  at the exit). The residence time for NG within the catalytic media was determined to be approximately 36 ms. Addition of some additives from TABLE I improves performance. For example, adding organic Saffron gives approximately 78% NG DRE ( $\approx 81.5\%$  at the reactor exit) for an NG inlet concentration of 10 ppmv but all other experimental conditions identical to that of the base-case test described above.

FIG. 12 depicts the laboratory flow reactor data of the EXAMPLES 8 to 12 for photocatalytic conversion of nitroglycerin in air. The plug flow behavior of the single-cell reactor of EXAMPLE 7 is depicted and indicates the validity of equations 32 and 33, described before. The quantum efficiency at the onset,  $\phi_0$ , for nitroglycerin vapors in air was estimated

from the laboratory data of EXAMPLES 8 to 12 as displayed in FIG. 12 to be approximately 25%. In EXAMPLE that follows a method for mitigating the coupling effect and thus permitting partial or full decoupling of  $\phi$  from  $x_m$  (or  $\delta_f$ ) is disclosed.

#### EXAMPLE 14

EXAMPLE 14 describes the preferred embodiments of the present invention for designing multistage catalytic media for both low-flux and high-flux applications. Let's consider a segmented photocatalytic, thermocatalytic or combined photo- and thermocatalytic media that will allow multiple contact between the contaminated stream and the catalyst. The catalytic media within a single-cell can be partitioned in a manner that either maximizes the quantum efficiency of the process or minimizes the pressure drop across the cell.

The underlying principles for designing multistage catalytic media are disclosed with reference to FIG. 13a that depicts a single multistage photo-cell 1300 having unequally partitioned media. In FIG. 13a, a longitudinal impermeable shell 1304 with inlet end 1302 and outlet end 1306 and UV lamp 1309 having protective sleeve 1308 are coaxially mounted. The first catalytic media 1310 inside the shell has one end 1312 connected to the inlet 1302 of the impermeable shell 1304 and an opposite end 1316 connected to the UV lamp sleeve 1308 at distance  $l_1$ . A second catalytic media 1320 has one end 1322 connected to inside the shell 1304 and an opposite end 1326 connected to the UV lamp sleeve 1308 at distance  $l_2$ . The third catalytic media 1330 is connected similarly at distance  $l_3$  and the  $n^{th}$  catalytic media 13n0 is connected at distance  $l_n$ . The length  $l_1$  of the first media is greater than the length  $l_2$  of the second media and so forth. Each media segment forms a different stage (*i.e.* stage 1, stage 2, stage 3, ..., stage  $n$ ). Fluid carrying contaminant A flows into inlet end 1311 of the first media 1310 through sides of first media to a space between the media 1310 and the impermeable shell

1304 and then similarly into the other media 1320, 1330, ..., 13n0, respectively until it exits from the outlet end 1306 of the impermeable shell 1304. Now, with reference to **FIG. 13a**, rewrite equation (32) in the following form:

$$\ln \delta_f \equiv -(a\phi_0 - r'_{AS})H \equiv -\frac{(a\phi_0 - r'_{AS})}{Q_1 C_{A0}}$$

or

$$Q_1 \equiv -\frac{(a\phi_0 - r'_{AS})}{C_{A0} \ln \delta_f} \quad (39)$$

Again,  $Q_1$  refers to the flow rate of contaminant stream through a simple, single stage catalytic media (also termed stocking or cartridge in the case of the low-flux application). For the more general case of a catalytic media having "n" unequal stages, equation (32) takes the following form:

$$\delta_{i+1} \equiv \delta_i \exp \left\{ \frac{-(a\phi_0 - r'_{AS})\lambda_{i+1}}{Q_n C_{A,i}} \right\} \quad (40)$$

Where:  $\delta_i \equiv \frac{C_{A,i}}{C_{A0}}$ ,  $\delta_{i+1} \equiv \frac{C_{A,i+1}}{C_{A0}}$ ,  $\lambda_{i+1} \equiv \frac{l_{i+1}}{L}$ , and  $Q_n$  denotes the contaminant flow rate within a photocell having n unequal stages (as in **FIG. 13a**). Combining equation (39) and (40), to get

$$\delta_{i+1} \equiv \delta_i \exp \left( \frac{\lambda_{i+1} \ln \delta_f}{\psi_n \delta_i} \right) \quad (41)$$

Where

$$\psi_n \equiv \frac{Q_n}{Q_1} \quad (42)$$

$\psi_n$  is a monotonic function of n and as  $n \rightarrow \infty$ ,  $\psi_n \rightarrow \psi_\infty$  asymptotically, where

$$\psi_\infty \equiv \frac{Q_\infty}{Q_1} \equiv -\frac{\ln \delta_f}{1 - \delta_f} \quad (43)$$

Equation (43) can be readily proved by first considering equation (36) and noting that as  $n \rightarrow \infty$ ,

$\lambda_i \rightarrow 1/n = \epsilon$ , thus

$$y(\varepsilon) = \frac{\delta_i}{\delta_{i-1}} = \exp\left(\frac{\varepsilon \ln \delta_f}{\psi_\infty \delta_{i-1}}\right)$$

Now, consider the Taylor expansion of the  $y(\varepsilon)$  in terms of  $\varepsilon$  as  $\varepsilon \rightarrow 0$ , and neglecting  $\varepsilon^2$  and all higher order terms, to get

$$y(\varepsilon) = \frac{\delta_i}{\delta_{i-1}} \approx 1 + \frac{\varepsilon \ln \delta_f}{\psi_\infty \delta_{i-1}} = \frac{\ln \delta_f}{n \psi_\infty \delta_{i-1}}$$

Then

$$\delta_i - \delta_{i-1} = -d\delta = \frac{\ln \delta_f}{n \psi_\infty}$$

But

$$\delta_i = \delta_0 - i d\delta = 1 - i d\delta$$

Likewise, for the  $n^{\text{th}}$  term to get

$$\delta_n = \delta_0 - n d\delta = 1 - n d\delta$$

But,  $\delta_n = \delta_f$ , and

$$d\delta = -\frac{\ln \delta_f}{n \psi_\infty}$$

Then

$$\delta_f = 1 + \frac{\ln \delta_f}{\psi_\infty}$$

Thus

$$\psi_\infty = -\frac{\ln \delta_f}{1 - \delta_f}$$

This is equation (43) noted before. In this equation,  $\psi_\infty$  is a function of  $\delta_f$  only, *i.e.* at a

given  $\delta_f$ , equation (43) sets the ceiling (upper limit) on the extent of the multi-stage reactor performance. In a way, full decoupling is possible only if the catalytic cartridge contains infinite number of reaction stages. For all other cases for which a finite number of partitions are made, only partial decoupling will be obtained.

It is easy to show that as  $n \rightarrow \infty$ , the apparent quantum efficiency of the process always

approaches  $\varphi_0$  (i.e.  $\varphi_\infty \rightarrow \varphi_0$ ). Combine equation (39) and (43) to get

$$Q_\infty = -\frac{Q_1 \ln \delta_f}{1 - \delta_f} = \frac{a\varphi_0}{(1 - \delta_f)C_{A0}}$$

Then

$$1 - \delta_f = \frac{a\varphi_0}{Q_\infty C_{A0}}$$

Also, from equation (29)

$$\eta_\infty = \frac{a}{Q_1 C_{A0}}$$

Then

$$1 - \delta_f = \varphi_0 \eta_\infty$$

Finally, from equation (20), written in terms of  $\delta_f$  (instead of  $x_m$ )

$$\frac{\varphi_\infty}{\varphi_0} = \frac{\left( \frac{d\delta_f}{d\eta_\infty} \right)}{\left( \frac{d\delta_f}{d\eta_\infty} \right)_{as \eta \rightarrow 0}} = \frac{-\varphi_0}{-\varphi_0} = 1$$

As discussed before, in equation (43),  $Q_\infty$  refers to the contaminant flow rate across the catalytic media having an infinite number of stages (or compartments). Also, equation (43) provides the upper limit of performance for a single-cell photocatalytic, thermocatalytic or combined photo- and thermocatalytic reactor.

Now, again, with reference to **FIG. 13a**, write

$$\frac{\delta_i}{\delta_{i-1}} = \exp\left(\frac{\lambda_i \ln \delta_f}{\psi_n \delta_{i-1}}\right) ; \quad i = 1 \text{ to } n.$$

Subject to following three constraints:

$$\lambda_1 + \lambda_2 + \dots + \lambda_n = 1; \quad \delta_0 = 1; \quad \delta_n = \delta_f$$

Then

$$\psi_n \equiv \frac{\ln \delta_f}{\sum_{i=1}^n \delta_{i-1} \ln \left( \frac{\delta_i}{\delta_{i-1}} \right)}$$

5 OR

$$\psi_n \equiv \frac{\ln \delta_f}{\ln \delta_1 + \sum_{i=2}^n \delta_{i-1} \ln \left( \frac{\delta_i}{\delta_{i-1}} \right)} \quad (44)$$

10 Subject to constraint:

$$\delta_n = \delta_f. \quad (45)$$

Here, the objective is to maximize the normalized throughput  $\psi_n \equiv Q_n/Q_1$  subject to the constraint of equation (45). A convenient method for solving an equation such as (44) subject to a restrictive condition such as equation (45) is by *Lagrange's method of undetermined multipliers*. Thus

$$\delta_i = \delta_{i-1} \exp \left( \frac{\delta_{i-1} - \delta_{i-2}}{\delta_{i-1}} \right); \quad i = 2 \text{ to } n \quad (46)$$

The values of the parameters  $\delta_1, \delta_2, \dots, \delta_{n-1}; \lambda_1, \lambda_2, \dots, \lambda_n$  and  $\psi_n$  are determined by trial-and-error as depicted by the flow chart of **FIG. 13b**. A computer code in "C" language is given in TABLE II for calculating the optimum (with respect to performance) partitioning ratios for a single photocell catalytic media of the present invention. Again, the procedure just described results in a catalytic media and reactor configuration that is optimal with respect to the DRE of the target species but not pressure drop across the catalytic reactor.

TABLE III depicts the partitioning ratios for the optimum-performance, single-cell, and multi-segmented media having up to 7 partitions (calculated for exit DRE of 99.5%). TABLE IV depicts the extent of performance improvement expected in a range of DREs (varying from



70 to 99.9999%) for optimum-performance multi-stage low- and high-flux media having up to 10 non-equal stages, where  $n$  denotes the number of single-cell partitions chosen. . In many applications, it is desirable to employ a media and reactor configuration that provides the least amount of pressure drop albeit at somewhat reduced overall system performance.

TABLE II

ns=10 a1guess=0.1 ntrial=100 j=2.5 nt=count(col(1)) col(2)=1-col(1)/100	'# of stages/partitions 'initial estimate of $a_1$ '# of iterations to determine $a_1$ 'exponent for rapid convergence, >2 'enter %DREs in column 1 ' $\delta_r$ values
<pre> for n=1 to nt do cell(3,n)=a1guess^j for nn=1 to ntrial do cell(ns+2,n)=cell(3,n) cell(ns+3,n)=cell(3,n) for i=4 to ns+1 do cell(i,n)=((cell(3,n))^(1-1/j))*(exp(cell(i-1,n)/(cell(3,n))^(1-1/j))-1) cell(ns+2,n)=cell(ns+2,n)+cell(i,n) end for cell(ns+2,n)=-ln(cell(2,n))*(cell(3,n))^(1-1/j)-cell(ns+2,n) for ir=ns+1 to 3 do cell(ir,n)=(ln(cell(ir+1,n)/(cell(3,n))^(1-1/j)+1))*(cell(3,n))^(1-1/j) end for cell(2*ns+5,n)=abs(cell(ns+3,n)-cell(3,n))/cell(3,n)*100 end for cell(3,n)=(cell(3,n))^(1/j) cell(ns+3,n)=cell(3,n) cell(2*ns+6,n)=cell(3,n) for i2=4 to ns+2 do cell(ns+i2,n)=exp(cell(ns+i2-1,n))-1 cell(ns+3,n)=if(i2=4,cell(ns+3,n),cell(ns+3,n)+cell(ns+i2-1,n)) cell(i2,n)=cell(ns+i2,n)/exp(cell(ns+3,n)) cell(2*ns+6,n)=cell(2*ns+6,n)+cell(i2,n) end for cell(2*ns+3,n)=-ln(cell(2,n))/cell(2*ns+6,n) cell(2*ns+4,n)=(1-cell(2,n))/cell(2*ns+6,n)*100 for i3=2*ns+2 to ns+3 do cell(i3,n)=cell(i3-ns,n)/cell(2*ns+6,n)*100 end for cell(2*ns+6,n)=100*cell(2,n) end for </pre>	

TABLE III

# of stages, $n$	$l_1/L$	$l_2/L$	$l_3/L$	$l_4/L$	$l_5/L$	$l_6/L$	$l_7/L$
1	1						
2	0.6636	0.3364					
3	0.4934	0.3291	0.1775				
4	0.3962	0.2957	0.1989	0.1092			
5	0.3245	0.2605	0.1978	0.1371	0.0801		
6	0.2768	0.2316	0.1870	0.1432	0.1007	0.0606	
7	0.2413	0.2077	0.1744	0.1415	0.1092	0.0778	0.0480

TABLE IV

# of stages $n$	% Destruction & Removal Efficiency (DRE)										
	99.9999	99.999	99.99	99.9	99.5	99	90	85	80	75	70
1	1	1	1	1	1	1	1	1	1	1	1
2	4.029	3.572	3.1	2.612	2.259	2.103	1.566	1.469	1.399	1.344	1.299
3	6.275	5.398	4.513	3.621	2.994	2.724	1.834	1.681	1.573	1.49	1.423
4	7.703	6.537	5.369	4.205	3.402	3.063	2.045	1.801	1.67	1.571	1.491
5	8.789	7.424	6.061	4.703	3.765	3.365	2.089	1.878	1.732	1.622	1.533
6	9.528	8.02	6.515	5.02	3.988	3.55	2.159	1.932	1.775	1.657	1.563
7	10.083	8.468	6.857	5.258	4.156	3.689	2.211	1.972	1.807	1.683	1.584
8	10.514	8.816	7.124	5.443	4.286	3.796	2.252	2.002	1.831	1.702	1.6
9	10.857	9.094	7.337	5.592	4.391	3.882	2.283	2.026	1.85	1.718	1.613
10	11.137	9.321	7.511	5.713	4.476	3.953	2.309	2.045	1.865	1.73	1.623
$\infty$	13.816	11.513	9.211	6.915	5.325	4.652	2.558	2.232	2.012	1.848	1.72

### EXAMPLE 15

The analysis presented in EXAMPLE 14 is repeated with the objective of minimizing the overall cell pressure drop instead of maximizing its performance. Again, the *Lagrange's method of undetermined multipliers* can be employed which results in a uniformly partitioned media configuration. In other words, a single-cell catalytic process having equipartitioned media stages, will have the lowest overall pressure drop than all the like ones but having unequal reaction stages. An analytical technique similar to that described in EXAMPLE 14 for the high-performance media and photoreactor design can be used also to determine the performance ( $\psi_n$ ) of a uniformly partitioned (equipartitioned) photocatalytic reactor as follows:

Consider the equipartitioned catalytic media of the photo-cell 1400 depicted in FIG. 14a that comprises a longitudinal impermeable shell 1404 with inlet end 1402 and outlet end 1406

and a UV lamp 1409 having protective sleeve 1408 coaxially mounted therein. The first catalytic media 1410 inside the shell has one end 1412 connected to the inlet 1402 of the impermeable shell 1404 and an opposite end 1416 connected to the UV lamp sleeve 1408 at distance  $L/n$ . A second catalytic media 1420 has one end 1422 connected to inside the shell 1404 and an opposite end 1426 connected to the UV lamp sleeve 1408 at distance  $L/n$ , as well. The third catalytic media 1430 is connected similarly at distance  $L/n$  as well as the  $n^{th}$  catalytic media 14n0, which is also connected at distance  $L/n$ . The length of all partitioned media stages are equal to one another. Each media segment forms a different stage (*i.e.* stage 1, stage 2, stage 3, ..., stage n). Fluid carrying contaminant A flows into inlet end 1411 of the first media 1410 through sides of first media to a space between the catalytic media 1410 and the impermeable shell 1404 and then in a like manner into the other media, *i.e.* 1320, 1330, ..., 13n0, respectively until it exits from the outlet end 1406 of the impermeable shell 1404. Now, with reference to

**FIG. 14a**, and noting that:  $\lambda_1 = \lambda_2 = \dots = \lambda_i = \dots = \lambda_n = 1/n$ , write

$$\frac{\delta_i}{\delta_{i-1}} = \exp\left(\frac{\ln \delta_f}{n \psi_{n,m} \delta_{i-1}}\right) ; \quad i = 1 \text{ to } n. \quad (47)$$

Subject to following restrictions:

$$\delta_0 = 1 \quad \text{and} \quad \delta_n = \delta_f$$

Sum both sides of equation (47) to get

$$\psi_n \equiv \frac{\ln \delta_f}{\ln \delta_1 + \sum_{i=2}^n \delta_{i-1} \ln \frac{\delta_i}{\delta_{i-1}}}$$

Also

$$n \psi_n = \frac{\ln \delta_f}{\ln \delta_1}$$

Then

$$\delta_i = \delta_{i-1} \exp\left(\frac{\ln \delta_1}{\delta_{i-1}}\right) ; \quad i = 2 \text{ to } n. \quad (48)$$

The system of algebraic equations above can be solved by trial-and-error according to the flow diagram of **FIG. 14b**. Equation (46) and (48) are the basis of all single-cell, multistage catalytic media design and optimization. TABLE V depicts the expected performance improvement,  $\Psi_n$ , for  $n$  equally segmented single photocell catalytic media (up to 10 equal stages) for a range of exit DREs varying from 70 to 99.9999%. The predicted performance improvement depicted above has been experimentally verified for a number of multistage ( $n= 1$  to 4) stockings and a multi-component waste stream containing nitroglycerine and acetone. It should be noted that the values given in TABLES III, IV and V are equally valid for any other combination of target compounds, apparent quantum yield of disappearance at the onset and inlet concentrations as long as no strongly adsorbed surface species are present. When the contaminant stream contains compounds such as plasticizers (*e.g.* di-n-propyladipate, diethylphthalate) or other similar compounds, the surface adsorption effects must be more rigorously accounted for and do affect results derived above.

TABLE V

# of stages $n$	% Destruction & Removal Efficiency (DRE)										
	99.9999	99.999	99.99	99.9	99.5	99	90	85	80	75	70
1	1	1	1	1	1	1	1	1	1	1	1
2	3.713	3.325	2.92	2.496	2.183	2.043	1.551	1.458	1.392	1.339	1.296
3	5.691	4.951	4.196	3.424	2.872	2.631	1.814	1.668	1.564	1.484	1.419
4	7.033	6.042	5.04	4.026	3.309	2.998	1.967	1.788	1.662	1.565	1.487
5	7.985	6.813	5.633	4.444	3.609	3.25	2.067	1.865	1.724	1.617	1.53
6	8.693	7.385	6.071	4.752	3.829	3.432	2.139	1.92	1.768	1.652	1.559
7	9.24	7.827	6.409	4.989	3.997	3.572	2.192	1.96	1.8	1.678	1.581
8	9.675	8.178	6.678	5.176	4.129	3.681	2.233	1.991	1.824	1.698	1.597
9	10.031	8.465	6.897	5.328	4.237	3.77	2.265	2.016	1.844	1.714	1.61
10	10.326	8.703	7.079	5.455	4.326	3.844	2.292	2.036	1.86	1.727	1.621
$\infty$	13.816	11.513	9.211	6.915	5.325	4.652	2.558	2.232	2.012	1.848	1.72

In a like manner, it can be shown that the results given by equation (46) and (48) will be applicable to the high-flux media and reactor configurations of this invention as well.

### EXAMPLE 16

This EXAMPLE demonstrates the preferred embodiments of the present invention for designing high flux reactors. FIG. 14c depicts the equipartitioned, multistage high-flux media and reactor configuration of this invention that can be analyzed in a manner analogous to the low-flux photosystem of FIG. 14a. FIG. 14c combines the multistage equipartitioned embodiments of FIG. 14a with the high-flux media and reactor configuration of FIG. 9b, where the multistage embodiment is substituted for the single-stage fluidized bed media of FIG. 9b. In FIG. 14c, fluid carrying contaminant A flows in the direction of arrow A into the rotating catalytic stages 1, ..., n-1, n from the dark side of the rotating media 1455, 1565, ..., 14n5, in a manner described in FIG. 9b before. In FIG. 14c, high-flux multistage rotating fluidized bed reactor 1440 has rotating stages 1450, 1460, ..., 14n0, where n equals the number of partitions or baskets, all rotating in unison about stationary lamp 30b placed within the quartz sleeve 30c, also rotating in unison with the baskets. Fluid carrying contaminant A flows into the inlet port 21 and passes under the closed end 1452 of the basket 1450 and through the round perforated side 1454 and through high-flux catalytic media 1455 (suspended in place by the combined but opposing action of centrifugal outward acceleration of the media particles and inward acceleration due to aerodynamic drag forces on the media particles) into inner lit space 1450 and out the circumferencial gap opening 1456 near lip 1453. After which the contaminant fluid streams into the second rotating stage/basket 1460 beneath the closed end 1462 through perforated side 1464 through catalytic media 1465 into the inner lit space 1460 and out of the circumferencial gap opening 1466 next to lip 1463. Final contaminant flow streams through basket stage 14n0, in a

like manner, having similar components 14n2, 14n4, 14n5, and out the exit port 14n6.

The multistage catalytic media and reactor design equations described in EXAMPLE 14 and 15 give the reactor performance in terms of a normalized throughput (with respect to that of a simple, single-stage catalytic media/reactor). The analytical results derived above and given in TABLE V for an equipartitioned single-cell photoreactor having "n" identical catalytic media or reaction stages are also applicable to a photosystem comprised of "n" identical series photocells. Results of TABLE V imply that a system of n series photoreactors or a single photoreactor having n segmented stages shall perform progressively better as the number of units in series or stages within a photocell, n, is increased. It is also clear from the discussion above that an optimized photocell and media of this invention will deliver slightly higher DRE than a comparable one with the same number of equal stages (compare results of TABLE IV and V).

It can be appreciated that depending on the number of reaction stages chosen (*i.e.* "n"), in certain applications, it may be better to accept a slightly lower performance by segmenting the catalytic media into equal length partitions than design for optimum performance. This is so because the multistage cell pressure drop increases quickly as the number of reaction stages, n, is increased. For the low-flux catalytic media (stocking) of the present work, the skin pressure drop can be calculated from Darcy's law for flow through porous media (*i.e.*  $\Delta P_i = k u_i$ ) as follows:

$$\frac{\Delta P_n}{\Delta P_1} = \psi_n \sum_{i=1}^n \frac{1}{\lambda_i} \quad (49)$$

In this equation  $\psi_n$  is given by equation (42) and  $\lambda_i = l_i/L$ , as before. The permeability factor, k, is primarily a function of the type of fabric material or media used, weight and weave density, as well as the catalyst type and loading density applied. For a typical low-flux media of the present invention such as super flannel fabric coated with Kemira, UNTI-908 TiO<sub>2</sub> at a loading density of about 10% by weight of the fabric,  $k = 0.075$  "H<sub>2</sub>O/(cm/s), approximately. **FIG. 15**

depicts the trade-off between performance (*i.e.* high DREs due to large number of media stages,  $n$ , chosen) and the corresponding cell skin pressure drop.

**FIG. 16** depicts the low-flux design of the double-stage catalytic stocking 1600. The double-stage stocking consists of two segments partitioned at approximately 66 and 34% of the total photocell length. This is critical for achieving optimum conversion at a designated DRE of 99.5%. Different partitioning proportions must be used if the target DRE differs from the value above. The new partitioning ratios can be derived using the computer program given in TABLE III.

Referring to **FIG. 16**, double-stage stocking embodiment 1600 includes inlet flange 1602 having an interior opening. A hollow impermeable wall shell 1610 (fabricated from any suitable material such as DuPont's TYVEK<sup>R</sup> for flexible media or hard metallic tube if rigid shell design) has one end 1612 tie wrap connected to the opening in inlet flange 1602 and a second end 1613 connected to one end 1627 of a last stage catalytic media 1628 (prepared as previously described). Opposite end 1626 of last stage catalytic media is tie wrapped to a perimeter edge of an exit flange 1604. Along central axis of shell 1610 is a UV lamp 1630 placed within a quartz or fused silica sleeve 1629. One of the lamp ends 1632 lies adjacent to the close end 1633 of the quartz sleeve 1629 which is adjacent an opening 1601 in inlet flange 1602. The opposite end 1634 of the lamp 1630 connects to power supply leads 1635 that make the connection via the open end 1603 of the quartz sleeve 1629. The open end 1603 of the quartz sleeve 1629 is held in place within the opening of exit flange 1604 through which the quartz cooling dip tube 1637 services the UV lamp 1630 within the quartz sleeve 1629.

A first stage permeable catalytic media 1622 has an inlet end 1621 tie wrapped 1612 around passageway opening 1601 of inlet flange 1602, and a second end 1623 tied to a first mid-portion 1631 of quartz sleeve 1629.

A last stage permeable media 1628 has an inlet end 1624 connected to the exit/second rim 1613 of shell 1610, and a second end 1626 tie wrapped to a perimeter edge of an exit flange 1604.

Referring to **FIG. 16**, contaminated stream A flows into inlet opening 1601 of inlet flange 1602 in the direction of arrow E1, and flows over quartz sleeve closed end 1633 and through side walls of first stage permeable media 1622 in the direction of arrow E2 to the airspace between first media 1622 and interior walls of impermeable shell 1610. Stream A then flows in the direction of arrow E4 through the side walls of last stage permeable media 1628 and out of the double-stage photocell of the subject invention in the direction of arrow E5.

### EXAMPLE 17

This Example demonstrates the application of a two-stage photocatalytic stocking (DSPCS). A DSPCS was fabricated and tested using the photoreactor of EXAMPLE 7. Again, the reagent solution used contained 5% by weight nitroglycerin in acetone as in EXAMPLE 13. The carrier gas was air heated to approximately 95°C and flowing at 15.5 SCFM (approximately 20.2 ACFM) through the mixing chamber 158 (**FIG. 11b**) and then into photocatalytic reactor 110 (**FIG. 11b**) of EXAMPLE 7. Concentration of NG in the gas-phase was approximately 9.6 ppmv. Again, the stocking was cotton flannel having an OD of about 3.8 inches. The stocking had 2 stages with proportions for stage 1, and 2 being approximately 67, and 33 percent of the total stocking length, respectively. The nitroglycerin DRE was determined at about 98.3% (99.99% at the exit). The average nitroglycerin residence time was calculated to be about 36 ms.

**FIG. 17** depicts the low-flux design of the triple-stage catalytic stocking 1700. The 3-stage stocking consists of three segments partitioned at approximately 49, 33 and 18% of the total photocell length. This is critical for achieving optimum conversion at a designated DRE of 99.5%. Different partitioning proportions must be used if the target DRE differs from the value above. The



new partitioning ratios can be derived using the computer program given in TABLE III.

Referring to **FIG. 17**, triple stage stocking embodiment 1700 includes inlet flange 1702 having an interior opening. A hollow impermeable wall shell 1710 (made from any suitable material such as DuPont's TYVEK if flexible design or hard metallic shell, *e.g.* aluminum or steel, if rigid design) has one end 1712 tie wrap connected to the opening in inlet flange 1702 and a second end 1714 connected to one end 1727 of a last stage catalytic media 1728 (prepared as previously described). Opposite end of the last stage catalytic media is tie wrapped to a perimeter edge of an exit flange 1704. Along central axis of shell 1710 is a UV lamp 1730 placed within a quartz or fused silica sleeve 1729. One of the lamp ends 1732 lies adjacent to the close end 1733 of the quartz sleeve 1729 which is adjacent an opening 1701 in inlet flange 1702. The opposite end 1734 of the lamp 1730 connects to power supply leads 1735 that make the connection via the open end 1703 of the quartz sleeve 1729. The open end 1703 of the quartz sleeve 1729 is held in place within the opening of exit flange 1704 through which the quartz cooling dip tube 1737 services the UV lamp 1730 within the quartz sleeve 1729.

A first stage permeable catalytic media 1722 has an inlet end 1721 tie wrapped 1712 around passageway opening 1701 of inlet flange 1702, and a second end 1723 tied to a first mid-portion 1731 of quartz sleeve 1729.

A second stage permeable media 1725 has an inlet end 1724 connected to an interior mid-wall portion 1713 of shell 1710, and a second end 1726 tie wrapped to a second mid-portion 1733 along the quartz sleeve 1729.

A last stage permeable media 1728 has an inlet end 1727 connected to the exit/second rim 1714 of shell 1710, and a second end 1750 tie wrapped to a perimeter edge of an exit flange 1704.

Referring to **FIG. 17**, contaminated stream A flows into inlet opening 1701 of inlet flange

1702 in the direction of arrow F1, and flows over quartz sleeve closed end 1733 and through side walls of first stage permeable media 1722 in the direction of arrow F2 to the airspace between first media 1722 and interior walls of impermeable shell 1710. Stream A flows in the direction of arrow F3 into inlet end 1713 of second stage permeable media 1725 and in the direction of arrow F4 through second stage media side walls 1725 and to the airspace between the second media 1725 and interior walls of impermeable shell 1710. Stream A then flows in the direction of arrow F5 through the side walls of last stage permeable media 1728 and out of the 3-stage photocell of the subject invention in the direction of arrow F6.

#### EXAMPLE 18

This EXAMPLE relates to test results for a three-stage photocatalytic stocking (TSPCS). The experimental conditions and procedure for this test were essentially identical to that described in EXAMPLES 13 and 17 except that air was heated to about 90°C and metered at 29.95 SCFM (38.2 ACFM) through the mixing chamber 158 (FIG. 11b) and into the photoreactor 110 (FIG. 11b) of EXAMPLE 7. Concentration of nitroglycerin in the gas-phase was 9.3 ppmv. The material of the stocking was cotton flannel (see EXAMPLE 13 & 17), having an OD of 3.75 inches. The stocking had 3 stages. The active length of stage 1, 2 and 3 were approximately 49, 33, and 18 percent of the total TSPCS length, respectively. Total volume of NG/acetone solution injected was approximately 160.1 ml. Total experiment run time was 81 minutes. The NG DREs varied between 75% and 87% (corresponding to exit DRE of 88% and 100%, respectively). The average NG residence time was calculated to be approximately 15 ms.

#### EXAMPLE 19

This EXAMPLE demonstrates the application of a 4-stage (equipartitioned) photocatalytic stocking (QSPCS). All experimental conditions and procedure for this case were

essentially same as EXAMPLE 18 except that air was heated to about 95°C and flowing at 40 SCFM (approximately 52 ACFM) through the mixing chamber 158 (FIG. 11b) and into the photoreactor 110 (FIG. 11b) of EXAMPLE 7. Concentration of NG in the gas-phase was about 9.55 ppmv. The material of the stocking was same as the EXAMPLES 13, 17 and 18 but having an OD of approximately 3.75 inches. Average UV light intensity on the inner surface of the QSPCS (at mid length) was measured (using ILC radiometer) to be about 2.06 mW/cm<sup>2</sup> (for  $\lambda=254$  nm). NG DREs varied between 68.4% and 81.5% (corresponding to exit DRE of 77% and 90%, respectively). Total NG residence time within the QSPCS was calculated to be approximately 10.8 ms.

The predicted values (from equations 39-48) for  $Q_n$  are plotted against the experimental values (from data of EXAMPLES 13, and 16 to 18) in FIG. 18. It can be seen that a good agreement is obtained between the predicted and measured values of  $Q_n$ . In general, the agreement between the predicted values and experimental data improves as the number of reaction stages is increased. There is also a large uncertainty associated with some of data as evident by the size of the error bars on the graph. Now, decoupling at module-level will be disclosed.

The benefits accrued from partitioning the catalytic stockings can be also realized by series arrangement of the single-cell reactors each containing a single-stage photocatalytic stocking. Therefore, the overall performance of a catalytic system comprised of many single-cell units will increase substantially by arranging all the unit cells in the system in series with each other. Again, the penalty to be paid for series arrangement of the photocells is the increased pressure drop through the unit. It is now understood that an increased photocatalytic system performance (*i.e.* higher target DREs) can result from either or combination of the following three design approaches:

- 1- Single-cell implementation of the multistage catalytic media.

- 2- Module-level arrangement of the single-cell reactors, in series with each other.
- 3- Unit-level arrangement of the individual sub-units or modules in series, together.

Clearly, as far as the unit-level design is concerned, the unit cells or single photocells of the photosystem can be arranged in a number of different ways. For example, it is possible to arrange all of the photocells in parallel. In this way, the incoming flow divides equally amongst all individual single-cell photoreactors (*i.e.* photocells or unit cells). Alternatively, the unit cells can be divided into smaller groups or banks that are plumbed to one another in series to form a cluster of parallel branches each containing two or more unit cells, in series. It should be clear from discussions above that the process DRE is a function of both  $\phi_0$  of the target contaminant and the manner in which the individual photoreactors (photocells or sub-units) and catalytic media within each photoreactor has been configured.

Now, the criteria for the design and engineering of complex photosystems that combine the module-level decoupling with the single cell-level (media-level) partitioning to achieve optimum photosystem performance are disclosed.

## EXAMPLE 20

This EXAMPLE describes the preferred embodiments of the present invention in the context of designing a double-bank, equipartitioned multistage series reactors. **FIG. 19a** depicts the configuration of one preferred embodiment of the present invention that has been reduced to practice as a full-scale photocatalytic pollution control unit (PPCU). **FIG. 19a** combines two equipartitioned multistage embodiments 1900 (Bank A) and 1900' (Bank B) in series. Depending on the volume of the flow to be treated by the process, concentration of the target species and ultimate DRE desired, Bank A and B may comprise one or several like photocells connected in parallel to each other. Also, Bank A 1900 can have n stages (at media-level) while Bank B has m

stages (at media-level), where  $n$  can be less than, equal to or greater than  $m$ , as later described in reference to **FIG. 20**. Now, with reference to **FIG. 19a**, for two equipartitioned multistage series photoreactors, for the upstream photocell or Bank A (*i.e.* 1900) having " $n$ " equal stages, write

$$\delta_i = \delta_{i-1} \exp\left(\frac{\ln \delta_f}{n \psi_{n,m} \delta_{i-1}}\right) ; \quad i=1 \text{ to } n.$$

For the downstream photoreactor (Bank B 1900') having a media with " $m$ " equal stages, write

$$\delta_i = \delta_{i-1} \exp\left(\frac{\ln \delta_f}{n \psi_{n,m} \delta_{i-1}}\right) ; \quad i=n+1 \text{ to } n+m.$$

Subject to constraints:

$$\delta_0 = 1 ; \delta_n = \delta_0 \text{ and } \delta_{n,m} = \delta_f.$$

Then

$$\ln \delta_1 = \frac{\ln \delta_f}{n \psi_{n,m}}$$

or

$$\eta_{n,m} = -\frac{\ln \delta_f}{\psi_{n,m}} = -n \ln \delta_1$$

and

$$\begin{cases} \delta_i = \delta_{i-1} \exp\left(\frac{\ln \delta_1}{\delta_{i-1}}\right) ; & i=2 \text{ to } n. \\ \delta_j = \delta_{j-1} \exp\left(\frac{n \ln \delta_1}{m \delta_{j-1}}\right) ; & j=n+1 \text{ to } n+m. \end{cases} \quad (50)$$

The system of algebraic equations above can be solved iteratively according to the flow chart shown in **FIG. 19b**.

In a like manner, **FIG. 19c** depicts the configuration of yet another embodiment of the

present invention. **FIG. 19c** combines two multistage embodiments 1300 (Bank A) and 1300' (Bank B) in series. Again, Bank A and B may comprise one or several like photocells connected in parallel to each other. Also, Bank A 1300 can have  $n$  unequally divided stages (at media-level) while Bank B has  $m$  unequally divided stages (at media-level), where  $n$  can be less than, equal or greater than  $m$ , as discussed below.

The most desirable configuration for a given application depends on the exit DRE required, maximum pressure drop allowed, economic, and other considerations. Furthermore, the number of partitions at the cell or media levels as well as the level of partitioning chosen within each bank greatly affects the photosystem performance. The optimization calculations have been carried out for a number of configurations involving different combination of the partitioning numbers  $n$  and  $m$  for photosystems of **FIG. 19a** and **19c**, with NG as the primary target contaminant at the inlet concentration of 10 ppmv. Typical results are given in **FIG. 20**. It can be seen that combining parallel and series interconnects results in a substantial process efficiency improvement. Results of **FIG. 20** indicate that the photosystem efficiency is higher when the number of partitioned media in the downstream bank in the module is larger than that in the upstream bank of the series. In other words, if  $nm$  denotes  $n$  stage media implementation at the upstream bank of the module and  $m$  stage media implementation at the downstream bank in the module, then  $nm$  arrangement will give considerably higher photosystem performance than  $mn$  arrangement, where  $n < m$ . It is interesting to note that even though  $nm$  arrangement gives higher photosystem performance than  $mn$  arrangement (when  $n < m$ ), both configurations will result in exactly the same pressure drop across the unit.

It can be appreciated that a large number of combinations incorporating the decoupling concept at the media-, module- and unit-levels are possible and not all can be mentioned and discussed here. Nonetheless, the methodologies developed in previous sections and described in

many EXAMPLES given above are sufficient to allow exact calculation of the results and benefits derived from any other arrangement not covered in this disclosure.

### EXAMPLE 21

This EXAMPLE describes a full-scale system design based on the concepts disclosed here that is reduced into practice by the subject inventor. This EXAMPLE demonstrates the application of a partially decoupled photocatalytic pollution control unit (PPCU) based on a multistage design implemented at all component levels, *i.e.* at media-, module- and unit-levels. With reference to FIG. 21a and 21b, the full-scale low-flux PPCU consists of two sub-units or modules 2100 and 2110 (FIG. 21a) or 2120 and 2130 (FIG. 21b), plumbed together, in parallel to each other. FIG. 21a shows a two-by-two series-parallel arrangement of equipartitioned multistage media (stockings) implementation. In FIG. 21a, fluid containing contaminant splits between two identical sub-units or modules 2100 and 2110. Each sub-unit or module consists of 32 photocells clustered together (not shown in FIG. 21a) in two banks of 16 photocells each. Thus, each module has two banks and wherein each branch comprised of two photocells in series (1900 and 1900' in module 2100 and 1900" and 1900''' in module 2110). In other words, PPCU is arranged so that each of the two parallel modules has two banks of 16 branched photocells each or 16 parallel branches (not shown in FIG. 21a). In this arrangement, the incoming flow into each sub-unit or module splits into parallel streams (branches) and passes through 16 photocells of the first bank (1900 and 1900') before entering the second bank of 16 parallel photocells (1900" and 1900'''). FIG. 21b depicts a configuration similar to FIG. 21a except that the partitioning at the cell-level comprises unequal multistage media segmentation. In principle, it is possible to have multistage, cell-level segmentation of both equal and unequal type in one unit or a module. In practice, other considerations (*e.g.* cost, inventory, maintenance and service of the unit, etc.) are likely to limit the

type and number of cell-level, module-level and unit-level multi-staging and rearrangements. **FIG. 21a**, with double or triple equipartitioned multistage stockings presents the most likely and practical PPCU configuration that can be implemented. It is important to note that the PPCU of **FIG. 21a** and **21b** was designed and intended to use multistage stockings. The PPCU light chamber was intended to be simple design and thus no inlet manifold (flow distributor) was envisioned to be required. This is justified because the use of multi-stage stockings with the unit mitigates the effect of flow non-uniformity normally present with the use of single-stage stockings.

## EXAMPLE 22

This EXAMPLE demonstrates the preferred embodiments of the present invention for designing high-flux photocatalytic, thermocatalytic or combined photo- and thermocatalytic reactors and media. The general layout of the multistage high-flux catalytic media and reactor configuration of the present invention at the single-cell level has already been described in **FIG. 9b**. Just as the low-flux system benefits from the module-level and unit-level decoupling, the high-flux system can also realize considerable performance boost by the series arrangement of the single-cell reactors. In other words, the overall performance of a high-flux catalytic system comprised of many single-cell units will increase substantially by arranging all the unit cells in the system in series with each other. Again, the penalty to be paid for series arrangement of the photocells is the increased pressure drop through the unit. In short, increased high-flux system performance can accrue from decoupling at the cell or media-level, module or bank-level and unit-level implementation and optimization.

The preferred embodiments and design of the high-flux catalytic media of the present invention is now disclosed with reference to **FIG. 22**. **FIG. 22** depicts a 2-stage high-flux version of the low-flux full-scale unit of EXAMPLE 17, described before. The high-flux catalytic media 2200 & 2205 useful for the practice of this invention are from the group of dual



function catalysts of the Type III (*e.g.* transparent co-gelled SiO<sub>2</sub>/TiO<sub>2</sub> aerogels) and Type V (*e.g.* cation modified zeolites and noble or base metal supported titania). These moderate temperature catalytic media (approximately 200-400° C) are most suited for the high-flux thermocatalytic and photocatalytic process engineering and reactor design applications.

5           The high-flux reactor design also follows the same guidelines described before for the low-flux reactor design and analysis. One preferred embodiment of the present invention for the high-flux reactor configuration that readily satisfies the decoupling requirements is rotating fluidized bed reactor 2210. **FIG. 22** depicts one preferred embodiment of this Invention. The unit comprises two rotating fluidized bed reactors 2215 & 2220, in tandem, which rotate in the direction of arrow R1 within a plenum vessel 2210. The baskets 2225 & 2230 rotate at high speed to hold catalyst particles within by the centrifugal action. The contaminant stream enters via perforated basket wall and distributor 2240 & 2245. The contaminated flow 2250 enters radially and exits axially, at the top 2255 and bottom 2260 of basket 2225 and 2230. High-flux lamps 2270 & 2275 (*e.g.* medium pressure mercury lamps such as Voltarc Tubes, Inc. UV LUX series lamps) are placed into the fused-silica sleeves 2280 & 2285 located at the middle, along the axis of the reactor, see **FIG. 22**. Two identical reactors 2225 & 2230 in series provide higher combined process efficiency due to partial decoupling effect, discussed before. The rotational speed of the baskets can be varied automatically to control catalyst carry over. This is particularly important in the case of transition metal aerogels as the bed material. Catalyst particles can be fed into the reactors through the injection tubes 2290 & 2295. The rotating beds 2230 & 2240 can be operated in either horizontal or vertical configuration. The type of catalytic media used in each reactor can be the same or different depending on the type of waste stream to be treated. Means can be provided for easy loading and removal of the bed materials. It is

possible to run the centrifugal reactor under either fluidizing or packed bed conditions. The reactor parameters can be readily modified to meet the requirements of the treatment process.

It is to be noted that the contaminated stream that can be treated with the methods of the subject invention can be a fluid such as but not limited to air, gas, liquid, combination thereof  
5 and the like. As noted before, the contaminated stream can contain solid and particulate matter.

Although some preferred embodiments show the direction of the stream containing contaminants in one direction, the invention can effectively operate with the contaminant flow through the opposite direction, *i.e.* through inlet end to outlet end, and vice versa.

It is to be understood that the disclosure above is meant to be representative of the techniques and methods most useful to the practice of this invention. Since many modifications to the main embodiments of the invention can be made without departing from the spirit and scope of the invention, it is intended that all matter contained in the above description and shown in the accompanying drawings shall be interpreted as illustrative and not in a limiting sense.

It is also to be understood that the following claims are intended to cover all generic and specific features of the invention herein described and all statements of the scope of the invention which, as a matter of language, might be said to fall therebetween. Particularly, it is to be understood that in said claims, features, ingredients or compounds recited in the singular are intended to include compatible mixtures of such ingredients wherever the sense permits.